NASA MEMO 3-9-59A

NASA MEMO 3-9-59A

NASA

MEMORANDUM

A WIND-TUNNEL INVESTIGATION OF THE STALL-FLUTTER CHARACTERISTICS OF A SUPERSONIC-TYPE PROPELLER AT POSITIVE AND NEGATIVE THRUST

By Vernon L. Rogallo and Paul F. Yaggy

Ames Research Center
Moffett Field, Calif.

NATIONAL AERONAUTICS AND SPACE ADMINISTRATION
WASHINGTON
May 1959

NATIONAL AERONAUTICS AND SPACE ADMINISTRATION

MEMORANDUM 3-9-59A

A WIND-TUNNEL INVESTIGATION OF THE STALL-FLUTTER CHARACTERISTICS OF A SUPERSONIC-TYPE PROPELLER AT POSITIVE AND NEGATIVE THRUST

By Vernon L. Rogallo and Paul F. Yaggy

SUMMARY

An investigation has been made utilizing a three-blade, 10-foot-diameter, supersonic-type propeller to determine propeller flutter characteristics. The particular flutter characteristics of interest were (1) the effect of stall flutter on a propeller operating in positive and negative thrust, (2) the effect of stall flutter on a propeller operating with the thrust axis inclined, and (3) the variation of vibratory blade shear stresses as the stall flutter boundary is penetrated and exceeded. Thrust and power measurements were made for all test conditions. Wake and inflow surveys were made, when appropriate, to define the thrust and torque distributions and the magnitude of the inflow velocity. Stress measurements were made simultaneously to obtain the propeller flutter and bending response.

It was found when operating both in the positive and negative thrust regions that, for most cases after the onset of flutter, the magnitude of the flutter stresses at first increased rapidly with section blade angle, β, after which further increases in β resulted in only a moderate increase or a reduction in stress. Thrust-axis inclination up to the limit of the tests (angle of attack of 15° and dynamic pressure of 40 psf) appeared to have no effect on stall flutter. The stall flutter stresses were found to be directly associated with the section thrust characteristics of the blades. The onset of flutter was found to occur simultaneously with the divergence of the section thrust variation with blade angle from linearity for stations outboard of the blade 0.8-radius station. The maximum flutter stresses appeared to be a function of the maximum section thrust obtained at or in the vicinity of the blade 0.8-radius station. In an attempt to correlate two-dimensional airfoil data with three-dimensional data to predict the stall angle of attack (divergence of the section thrust) of the blade sections, it was found that no consistent correlation could be obtained. Also, a knowledge of the inflow conditions appeared to be insufficient to account for differences in airfoil characteristics between the two-dimensional and the three-dimensional cases.

INTRODUCTION

Propellers suitable for high subsonic and transonic speed aircraft have blades with very thin airfoil sections. Blades which have thin airfoil sections are flexible both in bending and in torsion. To absorb the high power available from turboprop engines during take-off and early climb, these thin, flexible blades must often operate at blade angles above those at which blade-section stall would occur. The dynamic characteristics of the blades coupled with the required operating conditions is conducive to a blade flutter phenomenon in torsion termed stall flutter. Stall flutter has been so violent, in some cases, that the design was precluded by structural limitations.

Semiempirical methods for prediction of the stall flutter boundary (i.e., the operating conditions at which stall flutter will occur) have been developed. However, the general applicability of empirical methods is not evident unless they are based on an adequate understanding of the characteristics and mechanics of stall flutter. Some characteristics yet unknown and believed worthy of investigation are as follows:

1. The variation of vibratory blade stresses as the stall flutter boundary is penetrated and exceeded.

2. The effects of stall flutter on propeller operating characteristics.

3. The effects of blade twist, power input, design lift coefficient, solidity, number of blades, etc., on the stall flutter boundary.

4. The applicability of the results of scale-model tests to full-scale design.

To provide information for items 1 and 2, full-scale tests of a supersonic-type propeller have been made. The tests were made in the Ames 40- by 80-foot wind tunnel which, because of its large size relative to the size of the propeller, minimized tunnel-wall interference. The propeller was selected because its dynamic characteristics were such that the blades were susceptible to stall flutter over a wide range of blade angles and rotational speeds. Tests were made with the propeller operating at both positive and negative thrust with the thrust axis parallel to the wind stream. Tunnel airspeeds corresponded to a range from near zero through early climb or landing and rollout speeds. Tests were made also at positive thrust conditions with the thrust axis inclined to the wind stream for early climb speeds. Vibratory shear stress characteristics of the blades and thrust and power characteristics of the propeller before and during stall flutter were measured for all operating conditions. Inflow velocity and wake surveys were made for positive thrust conditions.

A correlation has been made of the onset of flutter as well as the maximum flutter stresses with measured aerodynamic data. In addition, an analysis has been made to determine the applicability of two-dimensional airfoil section data to predict the three-dimensional stall angle, defined as the divergence of the section thrust variation with blade angle from linearity.

NOTATION

b blade-section chord, in.

c_d section drag coefficient

c_l section lift coefficient

c_{l_α} two-dimensional lift-curve slope, per deg

c_t elemental blade-section thrust coefficient, $\left(\frac{dC_T}{dx}\right)$

c_q elemental blade-section torque coefficient, $\left(\frac{dC_Q}{dx}\right)$

C_P power coefficient, $\frac{P}{\rho n^3 D^5}$

C_Q torque coefficient, $\frac{Q}{\rho n^2 D^5}$

C_T propulsive thrust coefficient, $\frac{T}{\rho n^2 D^4}$

D propeller diameter, ft

J propeller advance ratio, $\frac{V_\infty}{nD}$

M_B blade-section Mach number

N propeller rotational speed, rpm

n propeller rotational speed, rps

P power input, ft-lb/sec

Q propeller torque, ft-lb

r radius to any blade section, in.

R	tip radius, in.
T	propulsive thrust, lb
t	maximum blade-section thickness, in.
V_∞	velocity of free-stream tunnel air stream, fps
V_I	inflow velocity at propeller plane induced by blade loading, fps
V_i	total inflow velocity at propeller plane, $V_I + V_\infty \cos \alpha_G$, fps
x	fraction of blade radius, $\frac{r}{R}$
α_B	blade-section angle of attack, deg
$\Delta\alpha_B$	maximum variation (first-order) of α, $\alpha_{max} - \alpha_{min}$
α_G	geometric angle of attack of the thrust axis, deg
β	section blade angle, measured from a plane perpendicular to the thrust axis, deg
$\beta_{0.7R}$	section blade angle at the 0.7-radius station
φ	geometric angle of advance, $\tan^{-1} \frac{V_i}{\pi nDx}$, deg
ρ	mass density of air, slugs/cu ft

MODEL AND APPARATUS

Dynamometer and Propeller

The propeller and test rig used for the investigation are shown in figure 1 as they appeared mounted in the 40- by 80-foot wind tunnel. The propeller was driven by two 1500 horsepower (3000 rpm) frequency-controlled electric motors coupled in tandem and connected directly to the propeller. The three-blade, 10-foot-diameter propeller used for the investigation was designated as Curtiss C636D-A3X. The blades, designated design number 109640, were solid dural and had symmetrical 16-series airfoil sections. The geometric characteristics of the blades are given in figure 2. This type of propeller has been termed "a supersonic propeller" since at the design cruise speed the blade airfoil sections are operating at supersonic speeds.

The propeller blade angle was controlled by remote operation of the standard integral pitch control mechanism contained in the C636 hub.

Instrumentation

The blades were instrumented with Baldwin-Southwark type SR-4-CB10 strain gages as shown in figure 3(a). The gage locations are shown in figure 3(b). All blades had bending gages at 20 inches from the thrust axis and shear (torsion) gages at 42 inches from the axis. These positions were those where the maximum vibratory stress had been calculated to occur and the readings from these gages provided the phase relation and relative stress level of the blades to each other. The master blade had additional bending gages at 30, 40, and 50 inches from the thrust axis to define the radial variation of the flatwise bending and an additional shear gage at 24 inches from the axis to identify the torsional mode. The output signals of the gages, appropriately attenuated, were simultaneously directly recorded on a Consolidated 36-channel, moving-coil-type oscillograph using type 7-218 galvanometer elements. Only the vibratory stresses were recorded; the steady stresses were eliminated by blocking condensers.

Propeller blade angle was measured by means of a potentiometer attached to the blade index head of the integral pitch-control mechanism of the propeller. The potentiometer output was recorded on a direct-reading Brown potentiometer modified and calibrated to indicate the blade angle in degrees.

The propulsive thrust of the model was measured by the longitudinal force scales of the wind-tunnel balance system.

Measurements of the flow field were made in both the wake of the propeller and just upstream of the propeller. The wake surveys were made by means of an eight-tube directional pitot-static rake located 19-3/8 inches aft of the propeller plane. The rake is shown in figure 1. From the readings of this rake, both propeller thrust and torque distributions were obtained. The inflow surveys were made by means of a rake composed of three static and three total-head probes. The probes were located 8-3/16 inches forward of the propeller plane and at the 0.38-, 0.58-, and 0.78-radius stations. This rake is also shown in figure 1. Both rakes were connected to multiple-tube manometers which were recorded photographically.

The power input to the electric motors was measured by standard polyphase, laboratory-type wattmeters. The wattmeters were calibrated in terms of propeller torque by suspending the test rig in a cradle which allowed torque measurement.

The rotational speed of the propeller was observed by means of a Berkeley electronic counter connected to a tachometer generator located in the motors. The speed was also recorded on the oscillograph record by means of a pulse which was generated once per revolution by an alnico magnet, attached to the propeller hub, passing a fixed coil on the test rig.

TESTS

Propeller Nonrotating Vibrational Characteristics

The fundamental torsional frequencies of the nonrotating blades were determined with the propeller installed on the test rig. The blades were excited by electromagnets. The force and frequency of oscillation of the magnetic fields were controlled by an electronic power supply incorporating an audio-oscillator. The frequency of each blade was measured with the excitation applied at that blade. The tests were made at a blade angle of 13.5° measured at the 0.7-radius station. The fundamental torsional frequencies were found to be 113.5, 112.5, and 113.2 cycles per second for blades 1, 2, and 3, respectively.

The decay technique was used to determine the damping characteristic of each blade (i.e., the excitation power was cut off abruptly and the decay of the amplitude of vibration was recorded on the oscillograph). From these records for a given amplitude of excitation, the logarithmic decrements, δ, were determined and found to be 0.0055, 0.0050, and 0.0051 for blades 1, 2, and 3, respectively.

Wind-Tunnel Tests

The range of test conditions is tabulated in table I. Because of model power and blade stress limitations, the propeller could not be operated over the entire propeller rotational speed and blade angle ranges for all tunnel airspeeds. The test conditions generally began just prior to the onset of stall flutter and the stall flutter boundary was penetrated to the maximum conditions permitted by stress and power limitations. A few runs were made also to determine the propeller operating characteristics beginning at a condition far removed from flutter and proceeding through the flutter boundary to the maximum blade stress permissible.

Two techniques were used to penetrate the stall flutter boundary. The first was to establish a constant propeller rotational speed and to vary the blade angle while a constant tunnel velocity was maintained. The second was to establish a constant blade angle and to vary propeller rotational speed while a constant tunnel velocity was maintained. The first technique was found to be the most satisfactory from an operational standpoint and was employed throughout most of the tests.

The data were all recorded simultaneously by photographing instrument panels and multitube manometers with cameras which were synchronized with the recording oscillograph.

REDUCTION OF DATA

The effect of blade instrumentation on the airloads and resultant stresses is believed to be small, since the results of previous investigations on full-scale propellers have shown that the agreement in magnitude of blade stresses in a fully instrumented blade and blades of limited instrumentation were within the accuracy of the measurements. Tests were made with and without the inflow survey rake, under as nearly identical conditions as practical, to determine the effect of the rake on the onset of flutter and on the magnitude of the flutter stresses. The rake appeared to have no effect on either the onset of flutter or the magnitude of the flutter stresses. No corrections for tunnel-wall interference have been made since the effects of tunnel-wall interference are believed to be small because of the large ratio of the tunnel cross-sectional area to the disk area of the test propeller.

Oscillograph Records

Since the complete strain-gage system had been calibrated in terms of stress per unit deflection of the recording galvanometers, the blade vibratory stresses could be obtained directly from the oscillograph records. One record was taken for each test condition. The average length of record was 60 inches and was recorded at a speed of 40 inches per second. The value of stress at any gage location for a given test condition was taken to be the maximum stress indicated on the oscillograph record for that condition. The frequency of the stress variation was obtained directly from the oscillograph records by means of timing lines spaced at intervals corresponding to 0.01 second.

Propeller Wake-Survey Data

Blade element thrust and torque coefficients were computed by the method given in reference 1. This method required measurements of total-head pressure and flow angle immediately aft of the propeller plane in the absence of the propeller and in the presence of the propeller. Previous investigations (ref. 1 and others) have shown this to be an acceptable means of measuring thrust and torque (it is realized that some error exists when the blade sections are operating at a stalled condition).

Propeller Inflow Data

The inflow velocity at the propeller disk was determined by linear interpolation between the value of velocity measured at the inflow rake and value of velocity measured at the rake in the propeller wake. This

procedure is believed to be in accordance with momentum theory. Both survey rakes were calibrated prior to the test. The data obtained at low forward airspeeds were found to be inaccurate, in particular at the outboard blade stations, because of high flow angles caused by the contraction of the inflow stream (the inflow survey tubes were not of the directional type). Thus, the data presented herein are for a forward speed range of 58.5 to 183.5 fps.

Force Test Data

The propulsive thrust is defined as the longitudinal force with the propeller operating less the longitudinal force with the propeller removed, both at the same tunnel air-stream velocity.

RESULTS AND DISCUSSION

The results of this investigation and discussion pertinent thereto will be divided into three main sections, (1) typical flutter stress characteristics at both positive and negative blade angles (included herein are presentations and/or discussions of blade phasing at flutter, flutter boundaries, wake-excited flutter, and the effects of thrust-axis inclination on flutter), (2) section thrust and inflow velocity characteristics as determined from survey rake measurements (included herein are correlations of the aerodynamic data with flutter stress data, and an analysis to determine the applicability of two-dimensional airfoil section data to the prediction of the three-dimensional stall angle), and (3) propeller performance characteristics as determined from the tunnel force scales and power measurements (these include absolute values of both thrust and power for a typical case at positive and negative thrust, in addition to the thrust and power coefficients for all test conditions of the investigation).

Flutter Stress Characteristics

Flutter at positive thrust.- The flutter stresses as presented herein apply to all of the blades for a given test condition, since, for all conditions of sustained flutter, all three blades exhibited very nearly identical flutter characteristics. This could be expected from the results of the nonrotating tests which indicated that the blades were dynamically similar. Typical vibratory shear stress characteristics for the case of positive blade angle operation are shown in figure 4 for near-zero tunnel velocity and at moderate tunnel velocities. Aside from the obvious effects of increasing tunnel velocity (i.e., causing the initial shear stress rise to occur at higher blade angles), the stress rise characteristics for all

tunnel velocities are similar for a given rotational speed. Note that for most constant rotational speed runs with the exception of those for which stress peaks could not be reached (limitations in power, allowable stress, etc.) the stress at first increased rapidly with β, after which further increases in β resulted in only a moderate increase in stress and in some cases a reduction in stress. It was noted during the test that at the first indication of vibratory shear stress there was no consistency in the response of the three blades. It often occurred that one blade was experiencing a low value of vibratory shear stress (less than ±1000 psi) when a second would suddenly trigger and experience a somewhat higher value of vibratory shear stress. The first indication of vibratory shear stress for all blades was depicted by a wave form sinusoidal in shape but having an apparent beat frequency. This pattern was neither of a constant amplitude nor of a constant beat frequency. As the control parameter (rpm or β) was further increased, the beating tended to disappear when the value of shear stress increased to the order of ±1000 psi. In general, this occurred at about the same time for all blades. Further increase in the control parameter resulted in higher levels of shear stress of nearly equal magnitude for all blades and the wave form of the oscillation was of a sustained amplitude.

It is of interest to note the marked difference in the stress rise characteristics for propeller speeds below 1200 rpm, in contrast to those at and above this value. A consideration of two-dimensional flow indicates that these stress characteristics might be expected. Although the mechanics of flutter are not precisely known, it is believed that the variation of the lift forces on an oscillating airfoil is dependent upon the relative length of the repeating vortex pattern in the wake of the airfoil as compared to the chord length (i.e., the number of chords that the vortex pattern moves downstream in one cycle of vibration defines, in part, the forces on the airfoil). A parameter describing the geometry of the flow field is commonly referred to as the "reduced frequency parameter" and is defined by

$$K = \frac{b\omega_\alpha}{V}$$

where

ω_α frequency of the vibration, radians/sec

b semichord, ft

V local air velocity, ft/sec

Investigations have shown that the critical mean angle of attack at which energy is absorbed from the air stream is a function of this parameter. It has been found convenient to use the reciprocal of the reduced frequency parameter to denote a flutter speed coefficient, λ, written as (ref. 2)

$$\lambda = \frac{V}{b\omega_\alpha}$$

Experimental results indicate that flutter will not occur, regardless of the airfoil angle of attack, if the value of λ is less than unity. For the case of the propeller this coefficient varies in value along the blade because of the differences in local air velocity. The value of λ for the rotational speeds below 1200 rpm (fig. 4) was generally less than unity over the major portion of the blade.

Flutter frequency and blade phasing.- The torsional frequencies of the blades during flutter were found to be near the values of the torsional natural frequencies obtained during the nonrotating tests. However, since all blades differed in frequency with respect to each other (maximum variation of frequency was from 109 to 114 cps) and drifting occurred for each blade, no phase relations could be established. It was noted that a phase shift as great as 180° often occurred within a period of three-tenths of a second. These results are not in agreement with those reported in reference 3, wherein definite phase relations were observed to occur.

Flutter boundaries.- The flutter boundaries based on a constant shear stress level of ±1000 psi, established from the data of figure 4 and other similar data of this investigation, are shown in figure 5. Included is the static flutter boundary established from the data obtained at the WADC Laboratory for the test propeller. The choice of a criterion by which to establish flutter boundaries is somewhat arbitrary. The constant stress level criterion was selected, based to a great extent upon the characteristics of the onset of flutter which were discussed previously. For the test propeller, a value of ±1000 psi shear stress was generally indicative of a transition from a varying amplitude of the shear stress to the first sustained value of stress encountered. Other investigators have also used ±1000 psi as a criterion for flutter boundaries for aluminum blades.

Wake-excited flutter.- During the tests, flutter at low blade angles was observed on several occasions. Flutter occurred for only two rotational speeds, however, namely 1400 and 1800 rpm. Typical stress characteristics are shown in figures 6 and 7(a). This phenomenon has been experienced previously on other propellers and also on the test propeller at the WADC Laboratory. Flutter occurring at low blade angles has been termed "wake-excited flutter." Wake-excited flutter was characterized by a sustained value of stress nearly equal in magnitude for each blade and having a definite blade phase relationship. All blades were in phase at 1800 rpm, and at 1400 rpm the blades were 120° out of phase with respect to each other. This phasing is in agreement with the phase criterion for torsional flutter as established in reference 3.

Flutter at negative thrust.- Typical vibratory shear stress characteristics for the reverse thrust regime are presented in figure 7. For a given forward velocity, the stress rise as blade angle is changed begins at nearly the same blade angle for all propeller rotational speeds whereas at positive thrust the blade angle corresponding to the onset of flutter is more definitely a function of rotational speed. The rate of stress rise during negative thrust operation begins as it did in positive thrust

operation and in general the stress variations are similar. After the stresses reached their maximum value, further decreases in blade angle up to the maximum test limit of -17.5° were accompanied by an appreciable reduction in the absolute stress level for a given rotational speed. This trend is of significance since the implication is that operation in the negative thrust regime is possible with a propeller having marginal flutter characteristics. Thrust characteristics in this regime will be shown subsequently.

Flutter at positive thrust with thrust axis inclined.- Because of the oscillatory variation of the blade angle of attack when the thrust axis is inclined, it would be expected that stall flutter would be induced at a lower propeller blade angle than it would for the uninclined case at the same operating condition. Further, results obtained on two-dimensional airfoil sections show that the hysteresis in the lift characteristics depends on magnitude and frequency of oscillations in the section angle of attack (ref. 4). This suggested that the oscillatory angle-of-attack variation induced by thrust-axis inclination could have a pronounced effect on propeller stall flutter. However, figure 8 shows representative results of tests with thrust-axis inclinations up to 15° and corresponding tunnel velocities as high as 183.5 fps which indicate little change in the stall flutter characteristics relative to the uninclined case. In order to gain an insight into why thrust-axis inclination was not influential in altering the flutter characteristics from the uninclined case, computations were made to determine the $\Delta\alpha_B$ variation (extreme α_B change in blade angle of attack around the disk) for a typical case. These computations were based on strip analysis procedure for the following conditions: rotational speed of 1600 rpm, blade angle of 30°, thrust-axis inclination of 15°, and a tunnel velocity of 183.5 fps. This condition was selected to provide an indication of the $\Delta\alpha_B$ variation for the test condition where the propeller blades were near the onset of flutter (±350 psi shear stress at zero thrust-axis inclination). The results obtained indicate a variation of $\Delta\alpha_B$ from 5.65° at the propeller 0.3-radius station to 0.75° at the 0.8-radius station. These high values of $\Delta\alpha_B$ are confirmed by the relatively large magnitude of the measured once-per-revolution vibratory bending stresses (±5000 psi). The values of $\Delta\alpha_B$ are of significant magnitude and suggest that the blade would be well into the flutter region during a portion of a revolution, while diametrically opposite this position the blade would be appreciably removed from the flutter region if stall flutter phenomenon occurred over a large portion of a blade. Thus, an explanation as to why thrust-axis inclination does not influence stall flutter cannot be made without associating the aerodynamic characteristics of the blade sections with the flutter characteristics. A study of the wake survey data to be discussed subsequently, for the uninclined case, revealed that for all propeller operating conditions investigated, only the outer portion of the blade (approximately 20 percent) exhibited stall phenomenon. As indicated above, $\Delta\alpha_B$ over this region would be less than 0.75° and of insufficient magnitude

to significantly alter the stall flutter characteristics. The tendency of the inner portions of the blade to remain unstalled at angles of attack far in excess of what would be predicted from two-dimensional airfoil data will be discussed in the latter part of this report.

Flow Surveys at Proximity of Propeller

Correlation of onset of flutter with measured aerodynamic data.- In order to obtain a correlation of the onset of flutter with the aerodynamic phenomena occurring during flutter, comparisons have been made of the section thrust coefficient obtained from wake surveys and the blade torsional stresses. These comparisons have been limited to a range of rotational speed from 1200 to 1800 rpm which is believed to be the range of greatest interest for the propeller diameter tested. This range is also above that wherein the effects of reduced frequency are of significance and below that wherein the effects of Mach number become significant. Typical results of the variation of the blade-section thrust coefficient with blade angle are shown in figure 9. It may be noted that the blade angle for onset of flutter, as indicated by the initial rise in shear stress in figure 4, very nearly corresponds to the blade angle at divergence from linearity of the thrust variation at the outboard sections for a given value of J (see fig. 9). The divergence at the 0.78 and 0.90 stations occurs simultaneously with the onset of flutter (little or no indication of stall occurred for stations inboard of the 0.64-radius station for all test conditions). This divergence is believed to be associated with flow-separation phenomena at or preceding blade-section stall. It appears then from the foregoing that stall flutter is dependent upon the aerodynamic characteristics of airfoil sections at or near the stall angle and that only a single outboard section need be considered in the prediction of stall flutter.

Correlation of the maximum flutter stress with measured aerodynamic data.- Comparisons of the section thrust coefficient with flutter stress variations indicate that the maximum flutter stress is associated with the maximum thrust of the blade sections. The stress level appears to reach its maximum value when the maximum thrust is obtained at or near the vicinity of the 0.8-blade-radius station. This correlation can be made by comparison of figures 4(e) and 9(a) and (b) for operating conditions at a moderate forward velocity and figures 4(a) and 10(a) for a case near zero forward velocity. For rotational speeds well within the flutter boundary extremities (i.e., 1200 to 2200 rpm) after the maximum thrust had been realized over the outer 20 percent of the blade, further increases in β generally resulted in a reduction in thrust and a nearly sustained or a reduced value of absolute shear stress.

Theoretical prediction of stall flutter.- The foregoing discussion intimates that the onset of stall flutter occurs with the stalling (deviation of the section thrust variation from linearity) of the outboard

sections of the propeller blade. On this basis, theoretical prediction of the onset of stall flutter would require a knowledge of the blade-section angles of attack at which stall will occur and the true angles of attack of the blade sections under operating conditions. It has been customary to use two-dimensional airfoil data to determine the angle of attack at which stall will occur on an operating blade section. To predict the true angle of attack of a blade section, the three air-stream components forming the angle must be known accurately as well as the live twist resulting from blade loading. These components are the free-stream velocity, the rotational velocity, and the inflow velocity induced by the propeller loading. The first two of these are measured directly. The third is a function of the circulation about the blade section and is generally computed theoretically.

Attempts to correlate predicted blade-section stall with experimental results have often failed. Generally, the results indicate the stall occurs at a blade-section angle of attack greatly different from that predicted. The two-dimensional lift curve has been presumed applicable to the blade section in three-dimensional flow where the effects of flow separation are not significant. If this is valid, the error could arise from two sources; inaccuracy of the method of computating the induced inflow velocities or inapplicability of the two-dimensional data to predict the three-dimensional characteristics where the effects of flow separation are significant.

If the measured values of inflow velocities are assumed correct, it is possible to evaluate the accuracy of the method of computation of the induced inflow velocities and the blade-section angles of attack resulting from these velocities. The values of inflow velocity which were measured are shown in figure 11 as a function of $\beta_{0.7R}$. The angle of attack of a blade section is defined as

$$\alpha_B = \beta - \varphi$$

where

$$\varphi = \tan^{-1} \frac{V_i}{\pi n D x}$$

Using the experimental values of V_i from figure 11 and the known rotational velocities, values of α_B were determined at the 0.38-, 0.58- and 0.78-radius stations. Representative results are shown in figure 12.[1]

[1]The blade angle at which zero angle of attack occurred was computed from the conventional velocity diagram on the assumption that the induced flow was zero (i.e., $\alpha_B = 0^\circ$ when $\beta = \varphi_0$ and $\varphi_0 = V_\infty/\pi n D x$). The curves of figure 12 were made to pass through this blade angle. Both measured and computed values of α_B were corrected for blade live twist.

Also shown are values of α_B, which were computed for the same conditions. These computations were made by use of the blade-element theory and the two-dimensional lift curves in figure 13(a) (primarily from ref. 5). The average lift-curve slope from $\alpha_B = 0^\circ$ to 6° was used.

For the 0.38 and 0.58 stations, where wake rake data showed the sections to be unstalled, reasonably good agreement existed between the slopes of the α_B variations calculated by use of two-dimensional lift-curve slopes and those calculated by use of measured inflow data. On this basis alone, it would be concluded that inflow calculations by the method used are valid. The lack of agreement at the 0.78 station could be expected since the wake rake data showed evidence of stalling at that station (the lift-curve slopes would not be applicable and the measured inflow velocities are somewhat questionable). To see if this disagreement could be reduced by consideration of the effects of flow separation, calculations of blade-section angle of attack were made by use of the two-dimensional airfoil lift from figure 13(a) rather than the low angle-of-attack lift-curve slope. The disagreement remained even with this presumably more refined calculation as shown in figure 12(c). More striking evidence of inability to account for flow separation effects when two-dimensional data were used was obtained when an attempt was made to predict the onset of blade-section stall. The gross errors involved in such calculations might be expected since figure 12 shows blade-section angles of attack as high as 18° at the inboard stations where the wake rake data indicated little or no evidence of stall to exist. However, to examine this comparison in more detail, calculations were made of local thrust as a function of blade angle for the three stations examined in figure 12. The calculations were made by use of experimental values of section lift and drag (fig. 13) and were carried through blade angles corresponding to maximum section lift. As shown in figure 14,[2] the calculated stall occurs at blade angles well below the measured values at the 0.38 and 0.58 stations and at blade angles above those measured at the 0.78 station. These characteristics are similar to those of the sweptback wing where the discrepancy has been blamed on spanwise flow. The above results imply that it may be difficult if not impossible to predict the blade angle at which section stall will occur if section characteristics based on two-dimensional airfoil data are used.

Propeller Aerodynamic Performance

No effect of flutter on propeller thrust and power characteristics was found, as can be seen by comparison of figures 4 and 15. It may be noted that, although the flutter stresses rise abruptly and obtain relatively high values with increasing β there is no discontinuity in either the thrust or power variations.

[2]The wake rake values of c_t at the 0.58-radius station were obtained by interpolating between values indicated by the wake rake tubes at stations 0.50 and 0.64.

Because of this apparent lack of effect of flutter on thrust and power characteristics, it was considered plausible to present all of the thrust or power performance data on a single plot. The thrust and power coefficients are presented in figure 16. This figure serves to show the ranges of test variables covered during the tests. In addition, the repeatability of the data is also indicated since these data represent values obtained during different phases of the tests with duplications of given test conditions.

CONCLUDING REMARKS

The results of the propeller stall flutter investigation indicate that stall flutter can be associated with the aerodynamic characteristics of the blade sections. The onset of flutter was found to occur simultaneously with the divergence of the section thrust variation with blade angle from linearity for sections outboard of the blade 0.78-radius station. The maximum flutter stress appeared to be a function of the maximum thrust obtained at or in the vicinity of the blade 0.8-radius station.

In regard to the prediction of stall by use of two-dimensional airfoil data, it was found that there was a definite lack of correlation between two- and three-dimensional data. The apparent differences in c_{l_α} for the two cases were found to be quite significant and the differences in section-stall angle of attack for the two cases were phenomenal. For example, where two-dimensional data would indicate stall to occur in the vicinity of 6° to 8°, the airfoil sections at the inboard sections of the blade were operating at angles of attack as high as 20° without appreciable stall. A knowledge of the inflow conditions appeared to be insufficient to account for differences in airfoil characteristics between the two- and three-dimensional cases.

It appeared reasonable, for the test propeller, to use the constant stress criterion to establish flutter boundaries since the first sustained value of stress appeared to occur at the same stress value (± 1000 psi) for all test conditions. The correlation of the flutter stress data with aerodynamic data obtained from wake surveys suggests that a flutter boundary representative of the onset of flutter could be more appropriate if based on thrust divergence rather than on a constant stress level or rate of stress rise, if such divergence could be predicted adequately. (It is assumed that the dynamics of the blade are such as to support flutter.)

Since no definite phase relationship between blades at flutter occurred for the subject investigation, with the exception of the case of wake-excited flutter, the results with respect to blade phasing at flutter are contradictory to previous tests (ref. 3).

Flutter appeared to have no influence on either thrust or power characteristics.

The trend found in the negative thrust region for the magnitude of the stress to reduce with increasing negative β after a maximum flutter stress was obtained may be of importance for propellers used as an airplane braking force. Further tests should be made over an extended negative β range to study this trend and also to determine the possibility of stress reduction by a rapid reduction of β.

Thrust-axis inclination up to 15° appeared to have no effect on stall flutter. An analytical study made to determine the $\Delta\alpha_B$ due to thrust-axis inclination together with a knowledge of the region of the blade stall from wake survey measurements indicated that the value of $\Delta\alpha_B$ over the stalled portion of the blade was of such a low magnitude as to be insignificant in altering the flutter.

Ames Research Center
National Aeronautics and Space Administration
Moffett Field, Calif., Nov. 8, 1958

REFERENCES

1. Reid, Elliott G.: Wake Studies of Eight Model Propellers. NACA TN 1040, 1946.

2. Baker, John E.: The Effects of Various Parameters, Including Mach Number, on Propeller-Blade Flutter With Emphasis on Stall Flutter. NACA TN 3357, 1955. (Supersedes NACA RM L50L12b)

3. Edwing, H. G., Kettlewell, J., and Gaukroger, D. R.: Comparative Flutter Tests on Two, Three, Four, and Five-Blade Propellers. R. & M. No. 2634, British, 1948.

4. Mendelson, Alexander: Effect of Aerodynamic Hysteresis on Critical Flutter Speed at Stall. NACA RM E8B04, 1948.

5. Borst, Henry V.: Propeller Performance Analysis Aerodynamic Characteristics NACA 16 Series Airfoils. Part I, Rep. C-2000, Curtiss-Wright Corp., Propeller Division (Caldwell, N.J.), Dec. 2, 1948.

TABLE I.- TEST CONDITIONS

V_∞, fps	α_G, deg	$\beta_{0.7R}$, deg	N, rpm
Near zero	0	18 to 42	550 to 2200
58.5	0	18 to 42	800 to 2000
88.5	0	18 to 42	800 to 2200
115.5	0	18 to 42	800 to 2200
143.8	0	19 to 42	800 to 2000
183.5	0	-17.5 to 42	1200 to 1800
Near zero	0	-17.5 to -10	550 to 2200
58.5	0	-17.5 to -2	600 to 1800
88.5	0	-17.5 to -8	600 to 1800
115.5	0	-17.5 to 2	600 to 1800
143.8	0	-17.5 to 2	600 to 1800
88.5[a]	10	18 to 42	600 to 1800
115.5[a]	10	22 to 42	800 to 1800
143.8[a]	15	21 to 42	1000 to 1800
183.5	15	23 to 40	1200 to 1800

[a]Data not presented for these conditions.

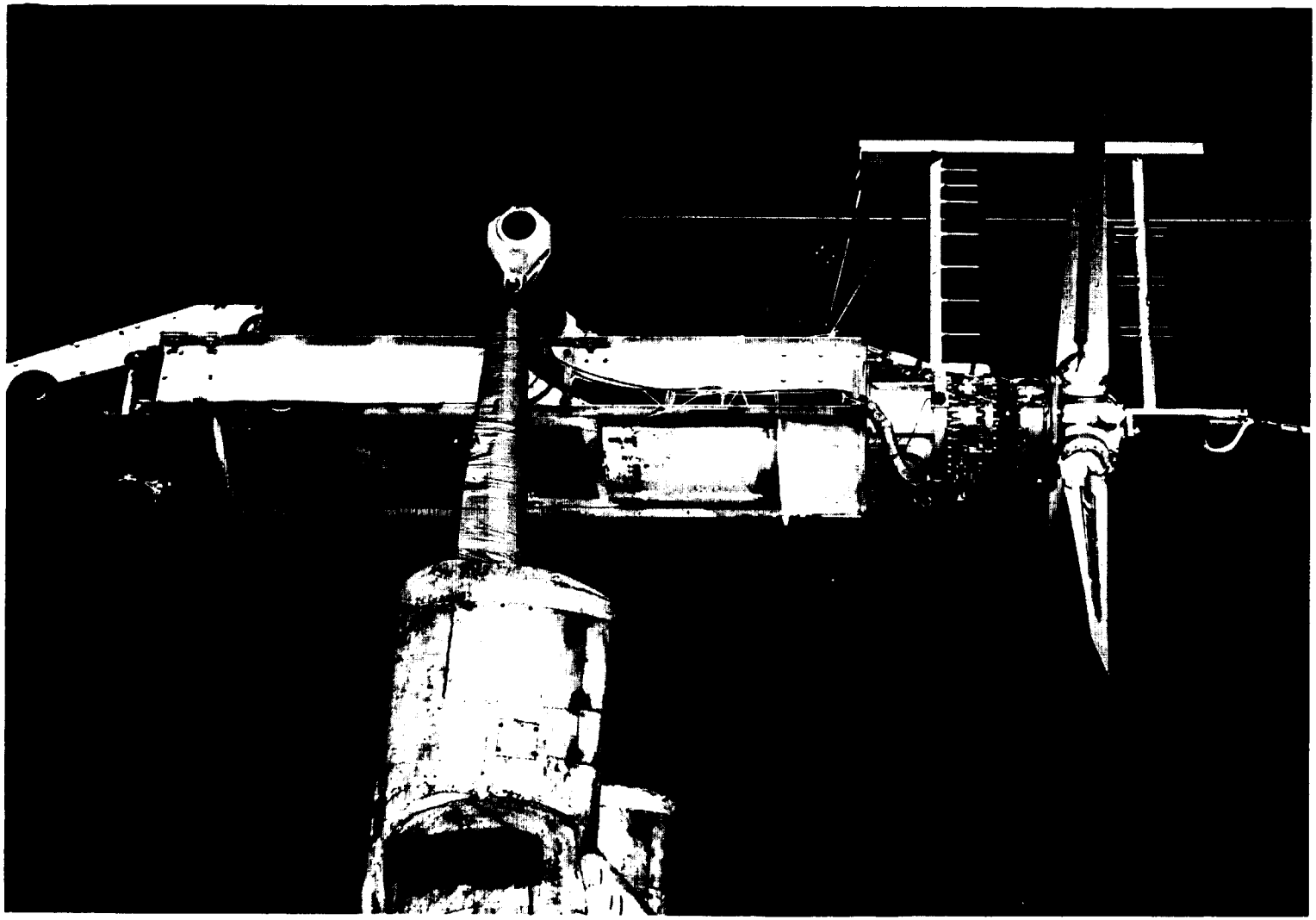

A-21672

Figure 1.- The propeller and test rig installed in the Ames 40- by 80-foot wind tunnel.

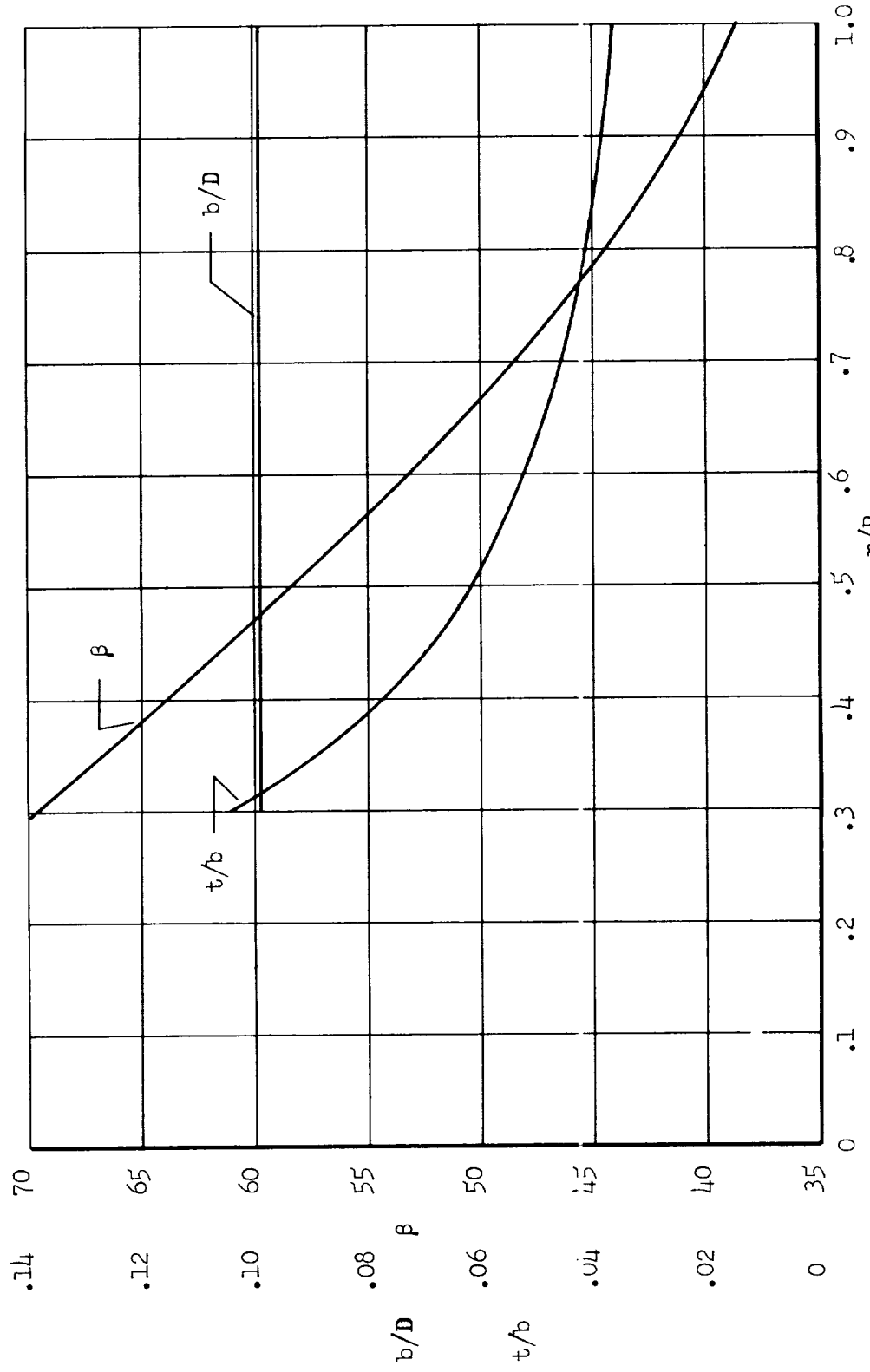

Figure 2.- Blade-form curves for the test propeller, Curtiss C636D-A3X; blade design 109640; diameter 10 feet.

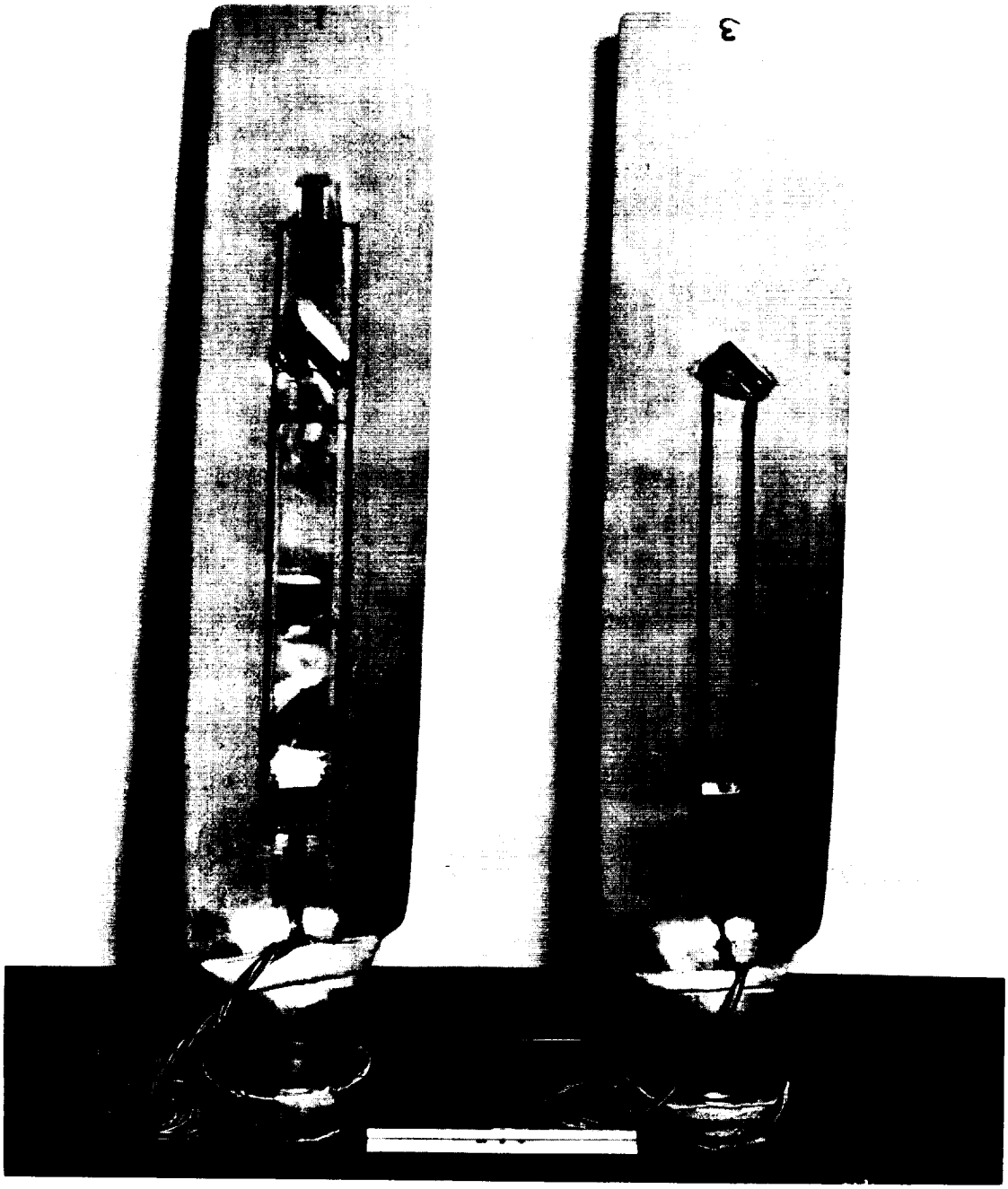

(a) Arrangement of strain gages on blade.

Figure 3.- Instrumentation of test propeller.

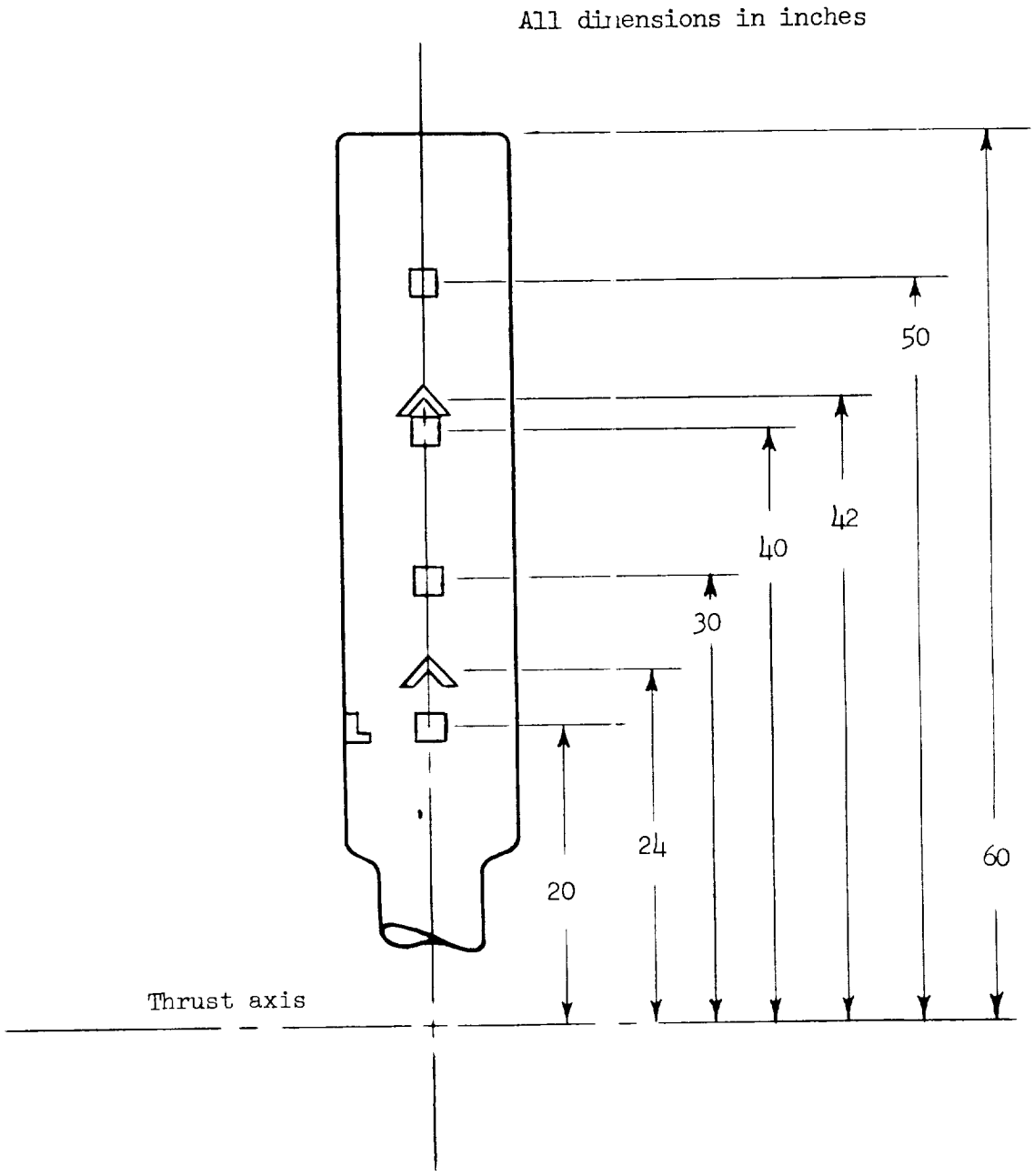

(b) Strain-gage location on fully instrumented blade.

Figure 3.- Concluded.

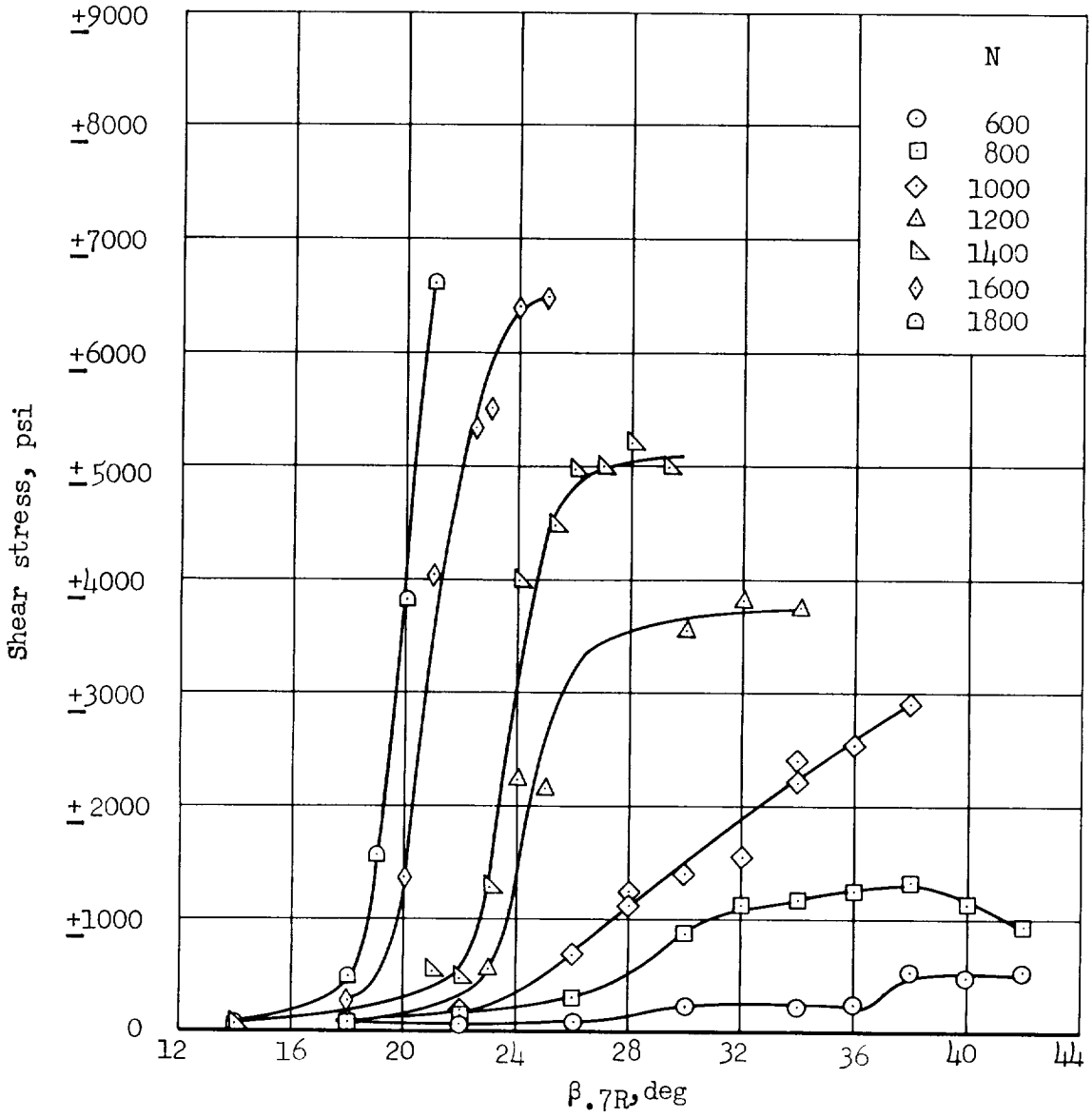

(a) $V_\infty \sim 0$ fps

Figure 4.- Flutter characteristics at positive thrust; $\alpha_G = 0^\circ$.

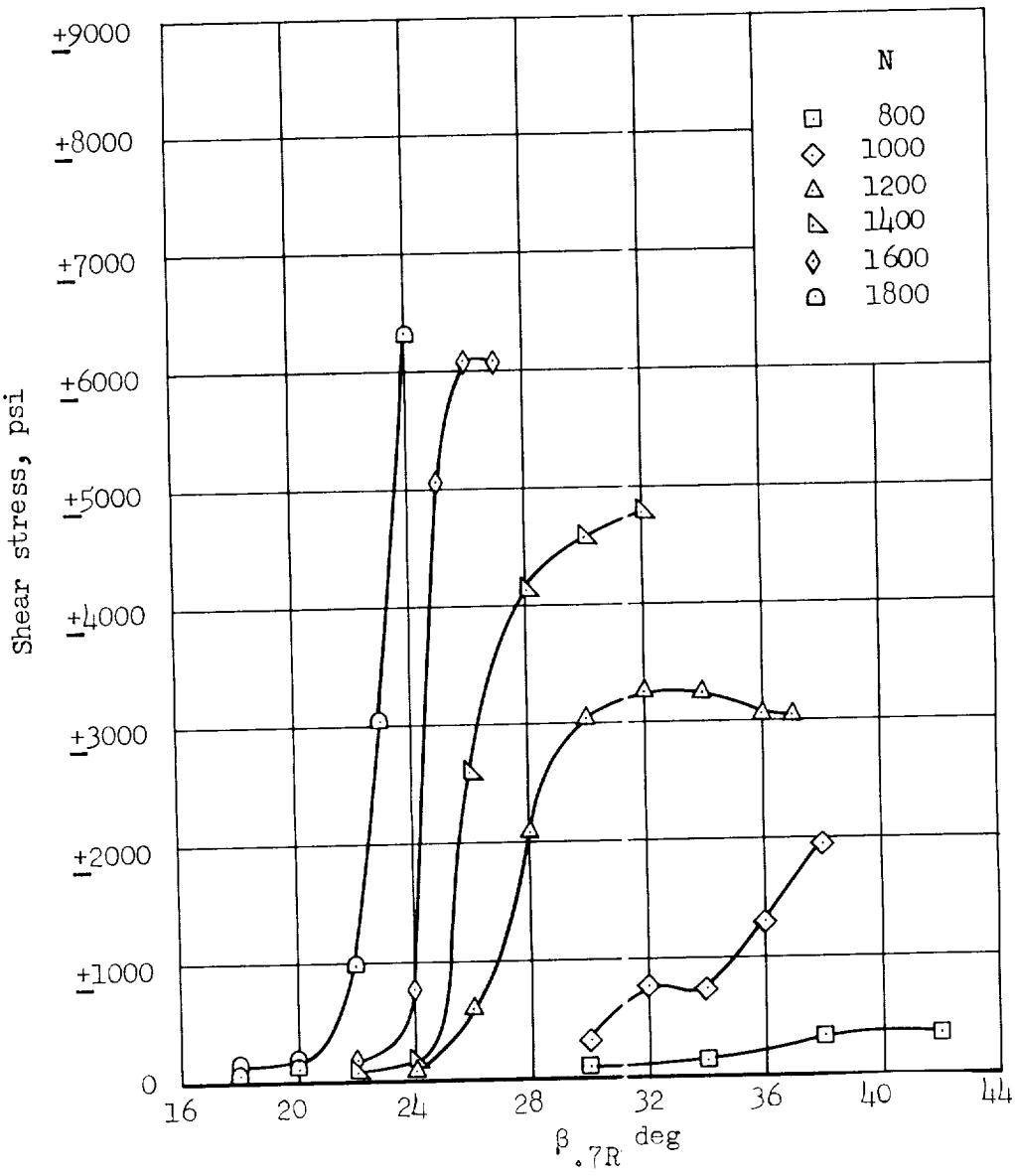

(b) V_∞ = 88.5 fps

Figure 4.- Continued.

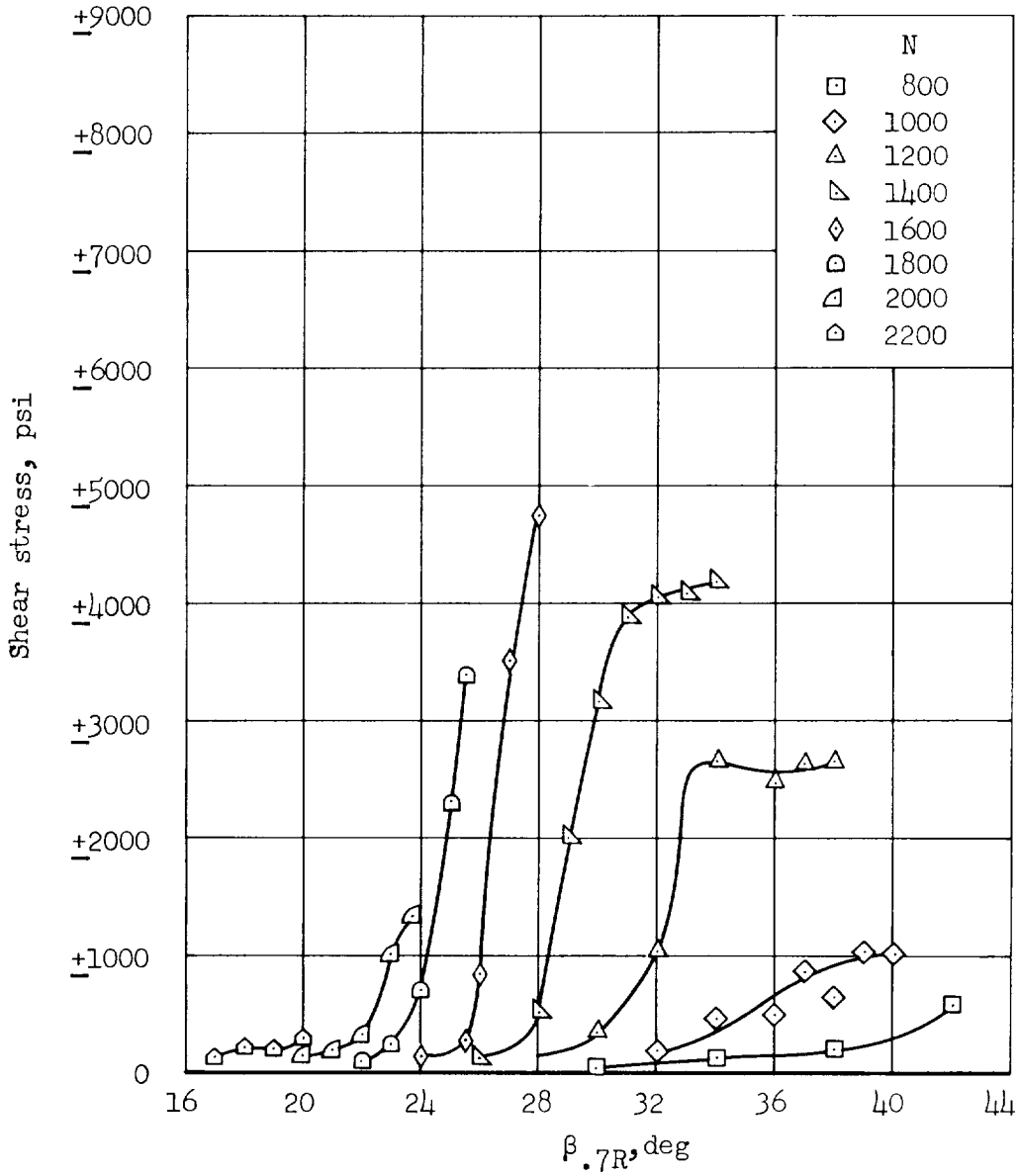

(c) V_∞ = 115.5 fps

Figure 4.- Continued.

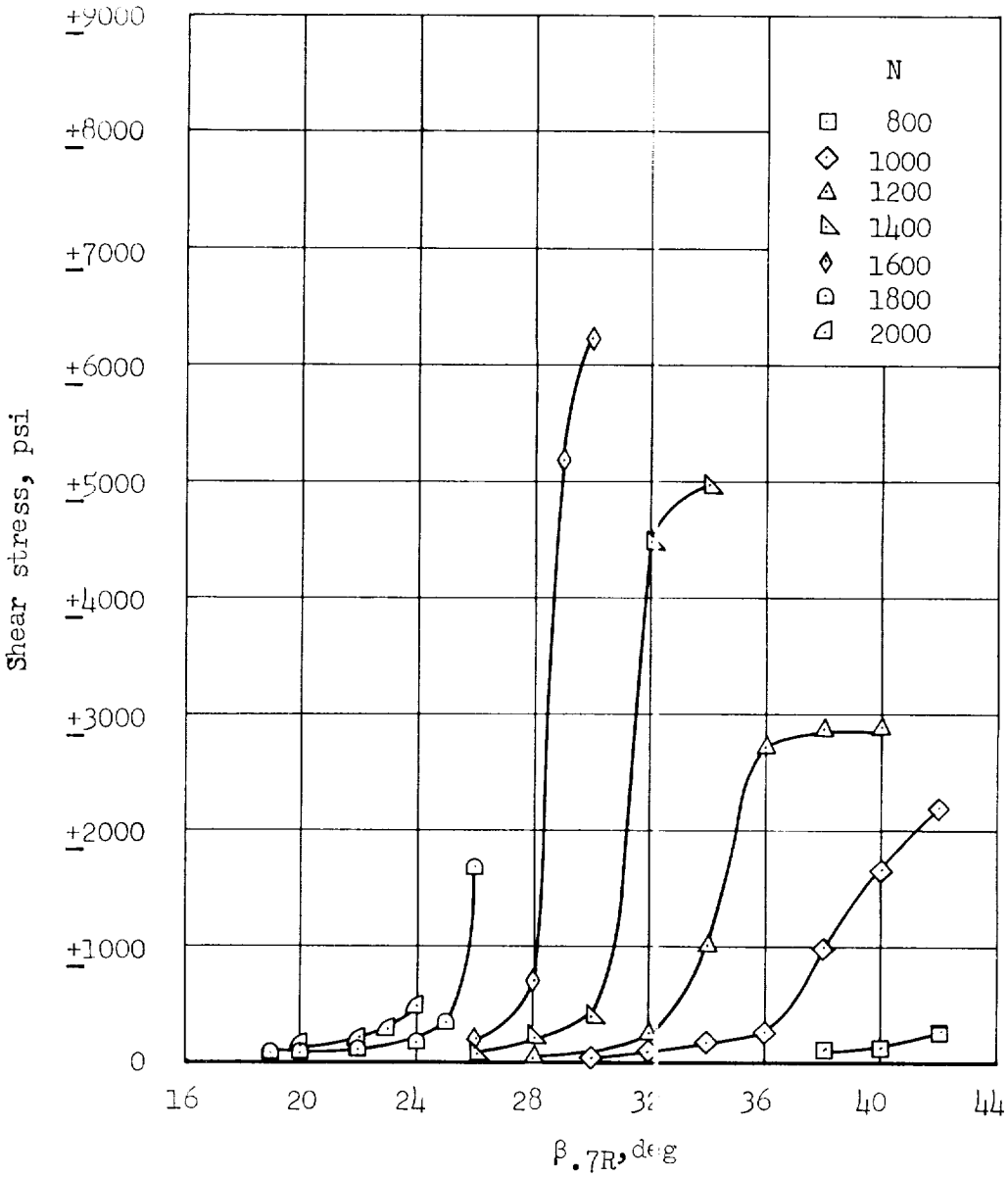

(d) V_∞ = 143.8 fps

Figure 4.- Continued.

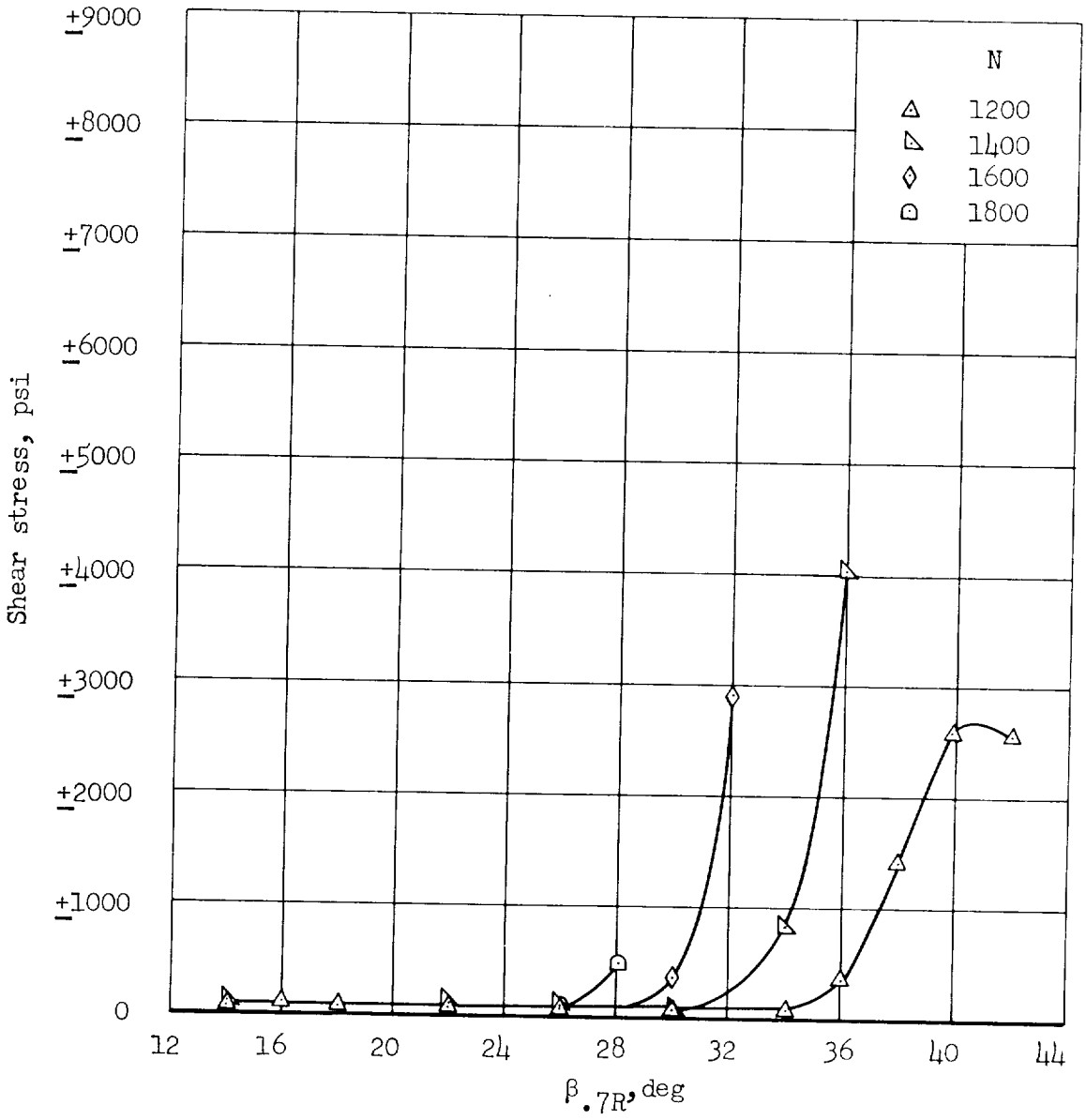

(e) V_∞ = 183.5 fps

Figure 4.- Concluded.

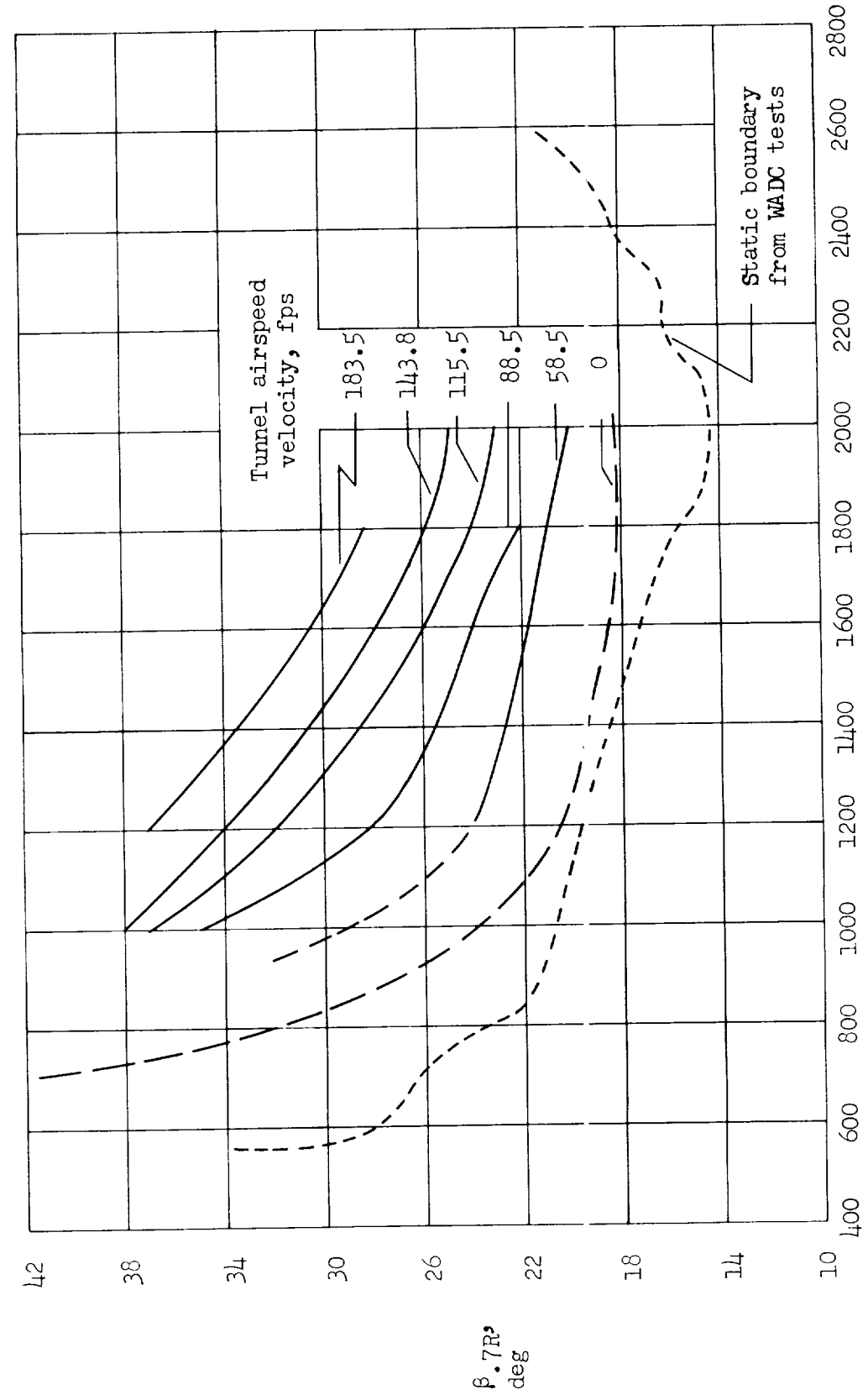

Figure 5.- Flutter boundaries for constant forward velocities; shear stress level criterion (±1000 psi); $\alpha_G = 0^\circ$.

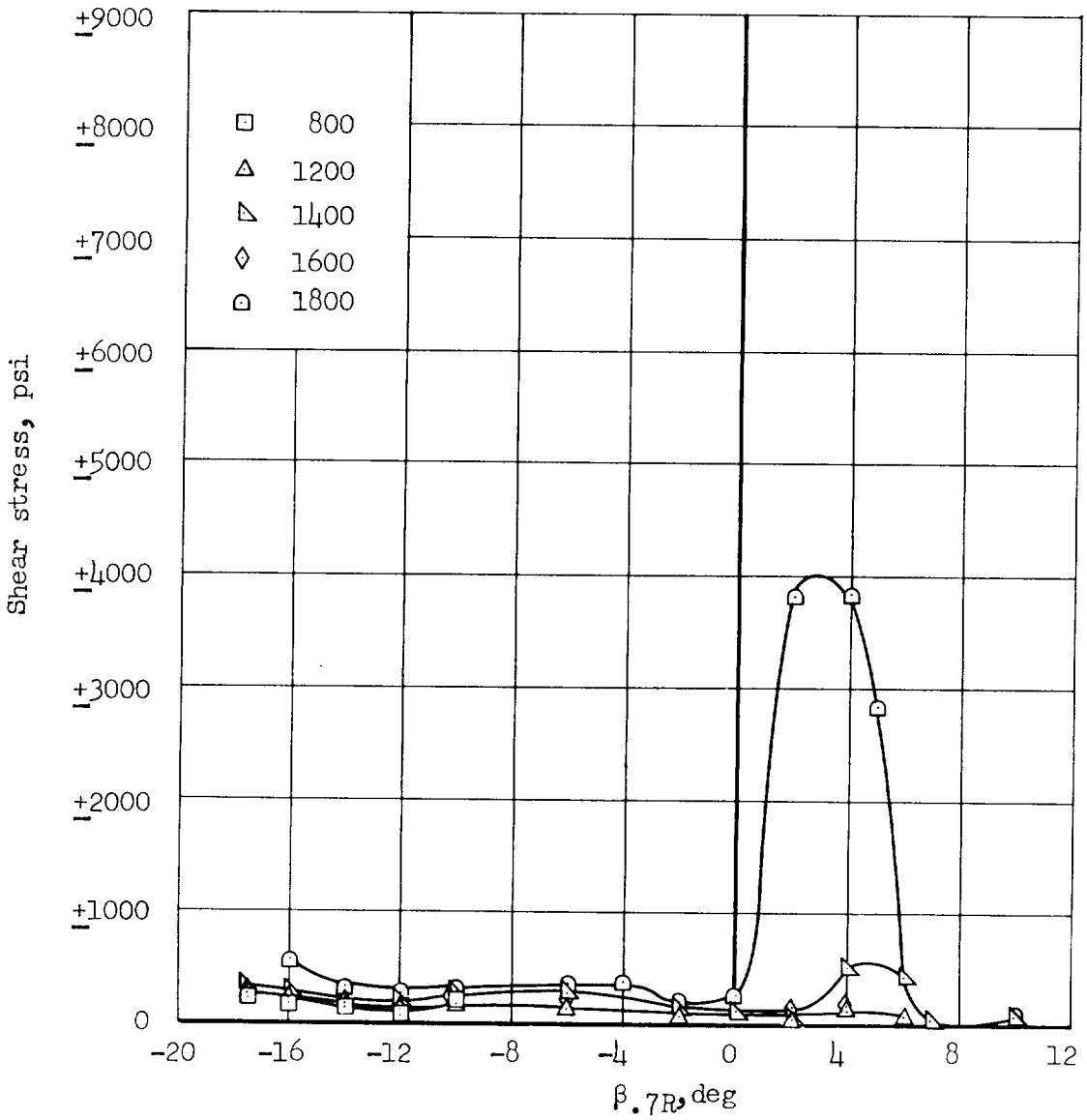

Figure 6.- Wake-excited flutter characteristics; $V_\infty \sim 0$ fps; $\alpha_G = 0^\circ$.

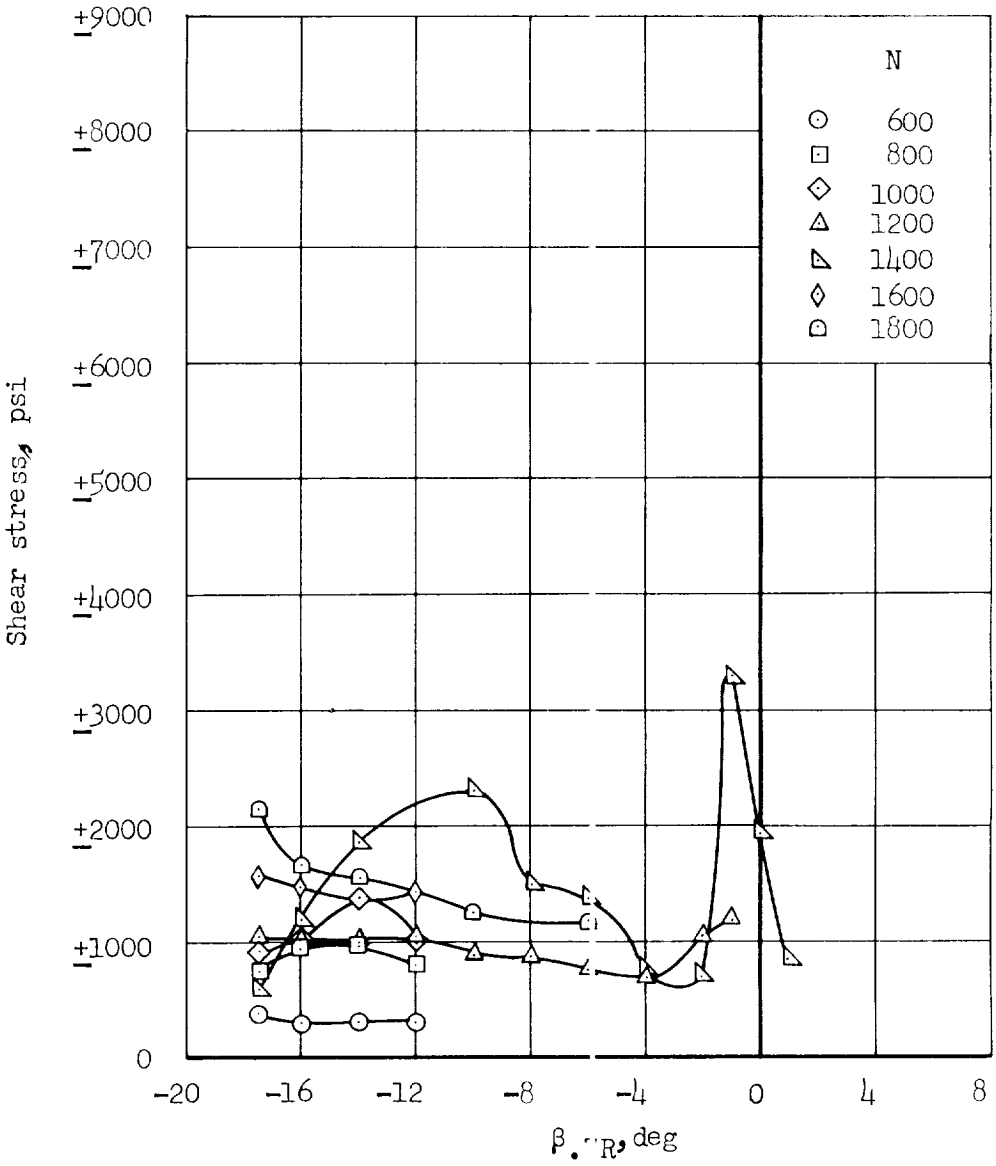

(a) V_∞ = 115.5 fps

Figure 7.- Flutter characteristics at negative thrust; $\alpha_G = 0^\circ$.

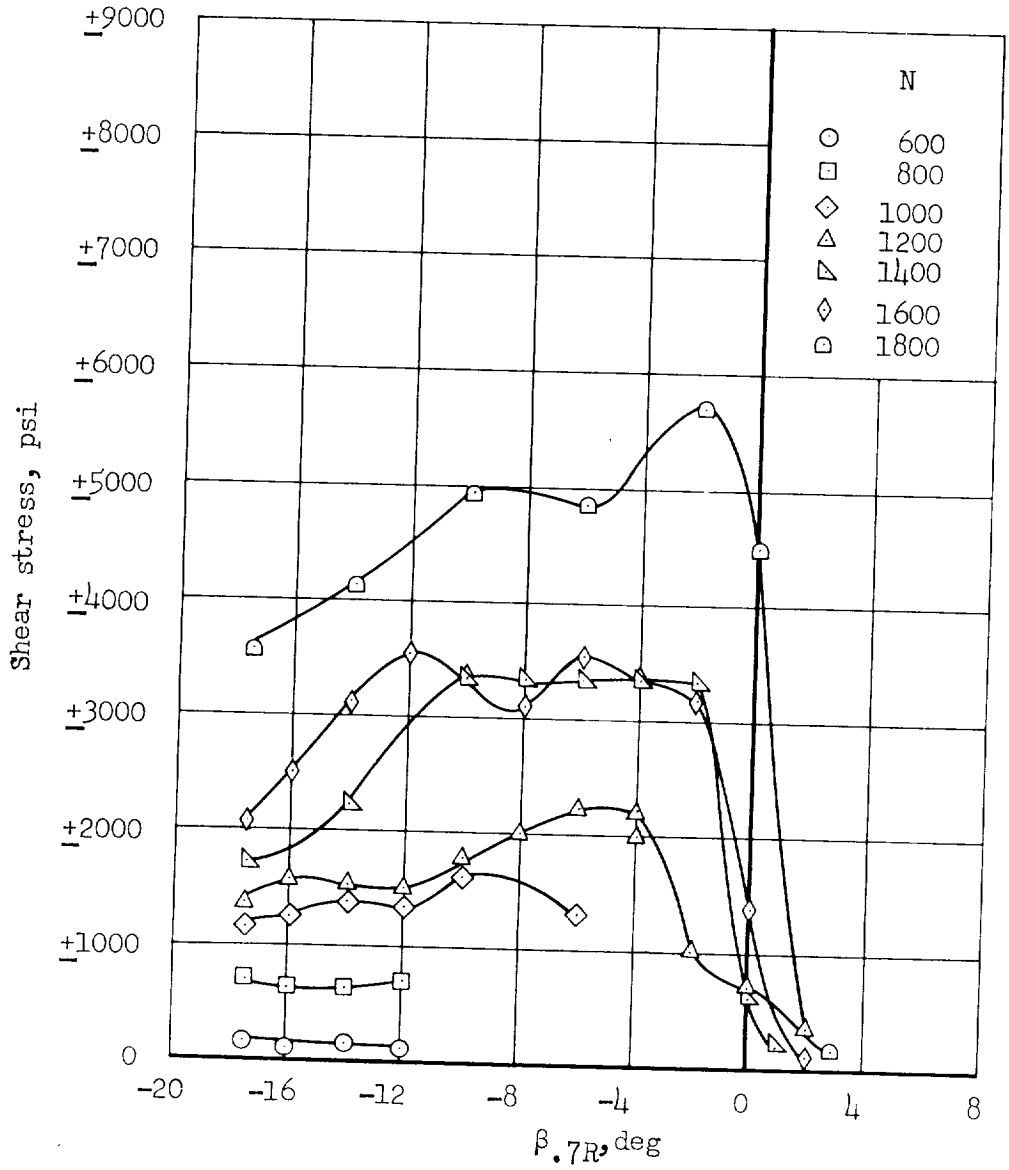

(b) V_∞ = 143.8 fps

Figure 7.- Continued.

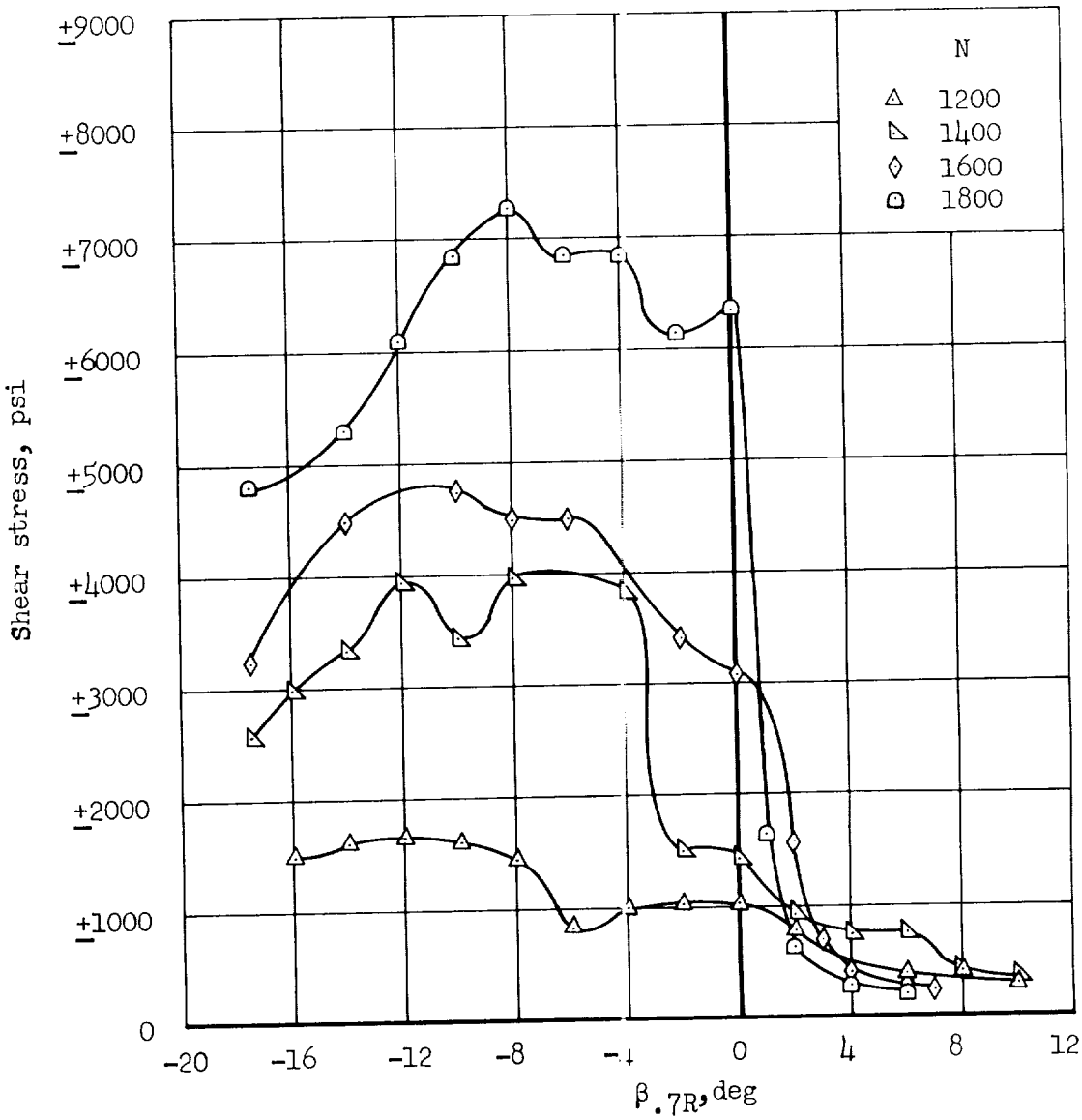

(c) V_∞ = 183.5 fps

Figure 7.- Concluded.

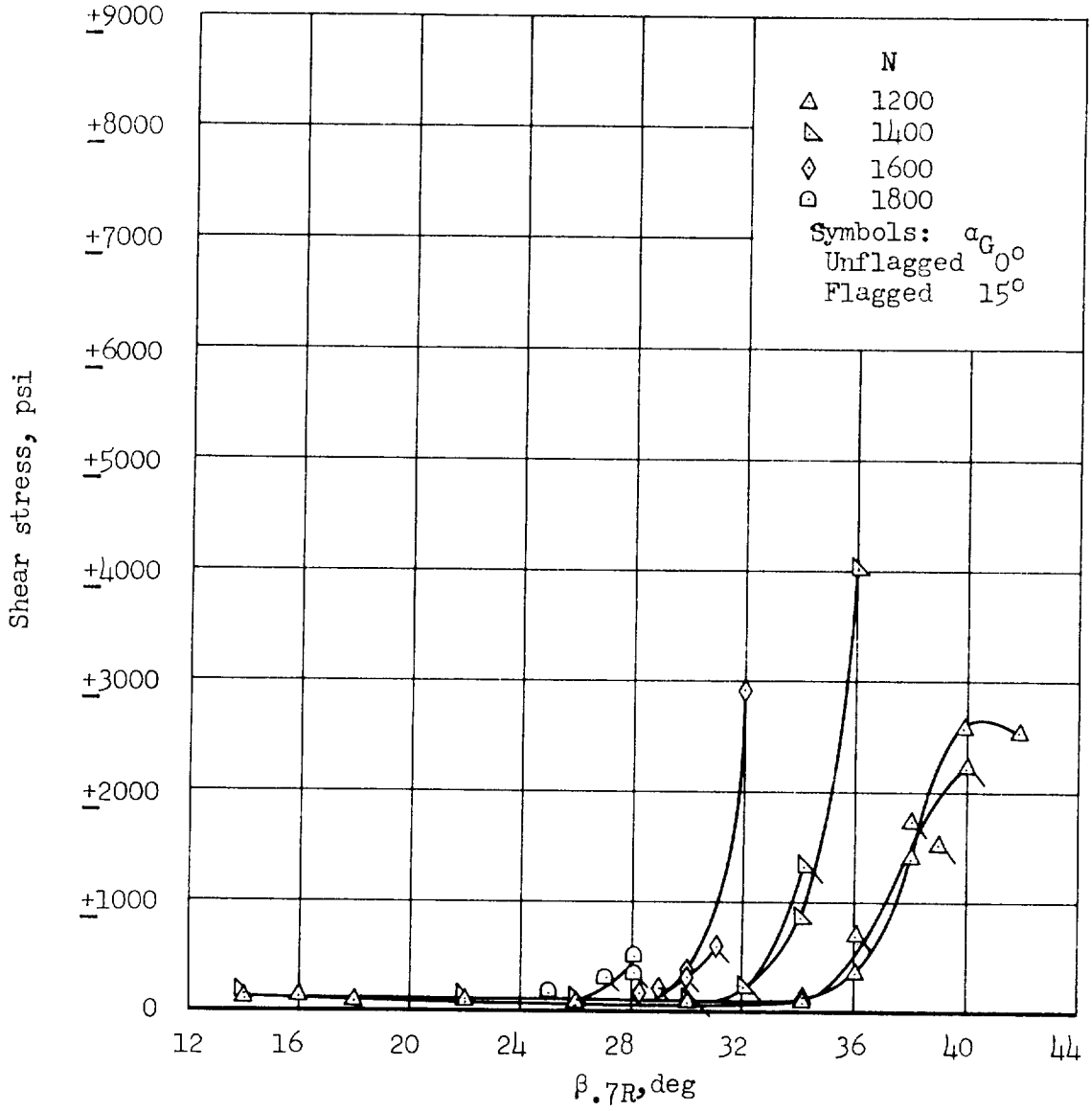

Figure 8.- Comparison of flutter characteristics at positive thrust with thrust axis inclined and noninclined; V_∞ = 183.5 fps.

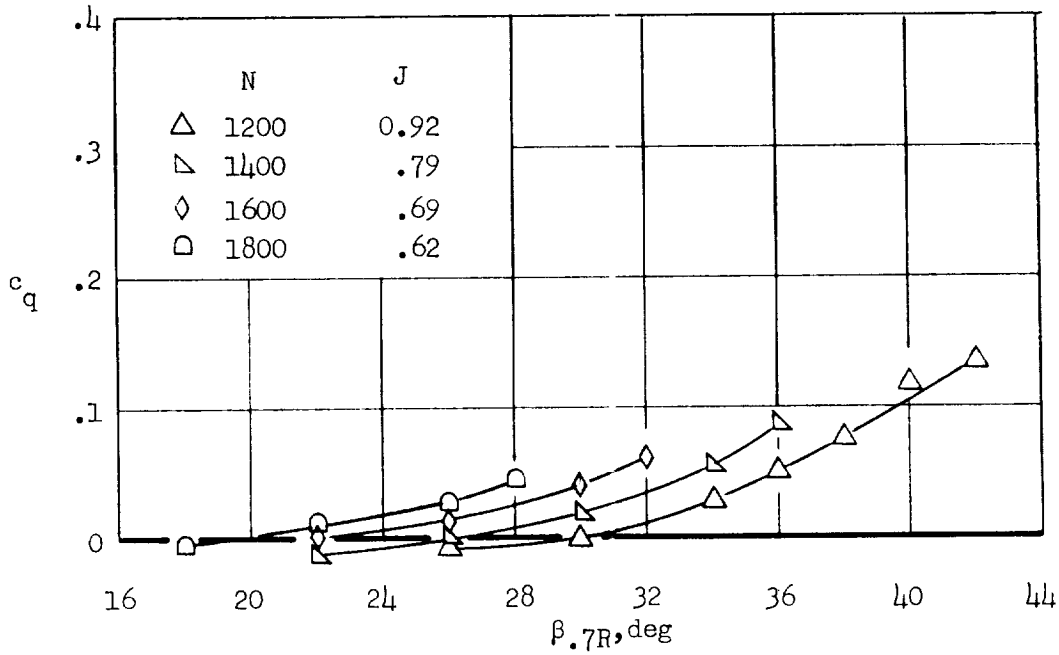

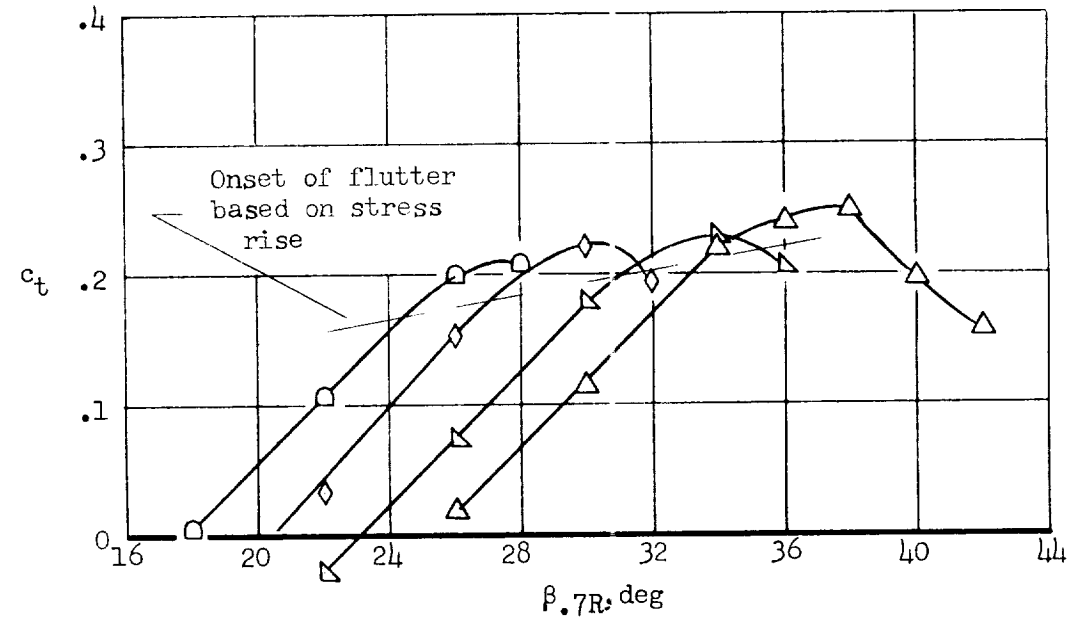

(a) Survey tube location; x = 0.90.

Figure 9.- Variation of measured section torque coefficient, c_q, and section thrust coefficient, c_t, with blade angle at V_∞ = 183.5 fps; $\alpha_G = 0^\circ$.

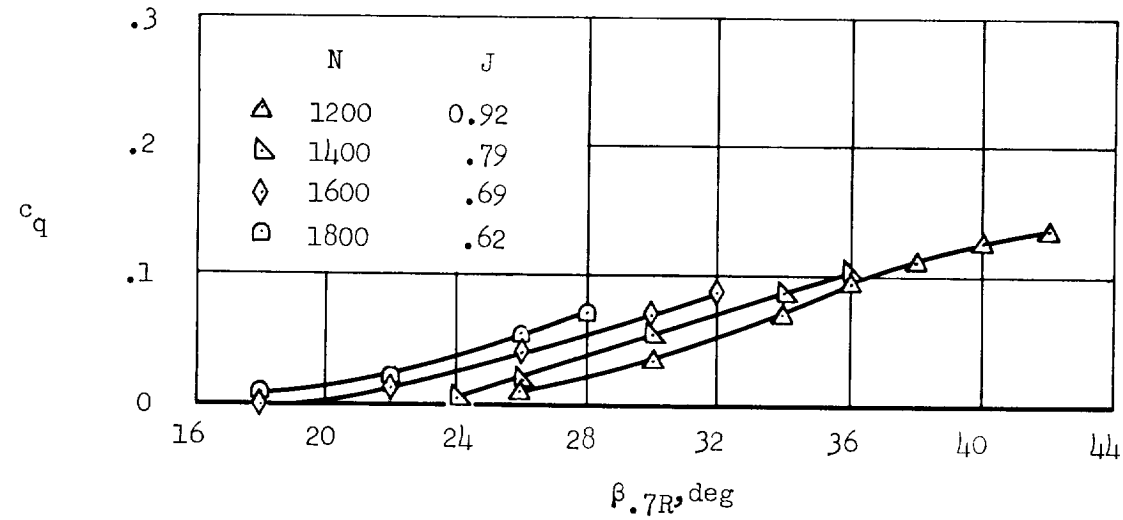

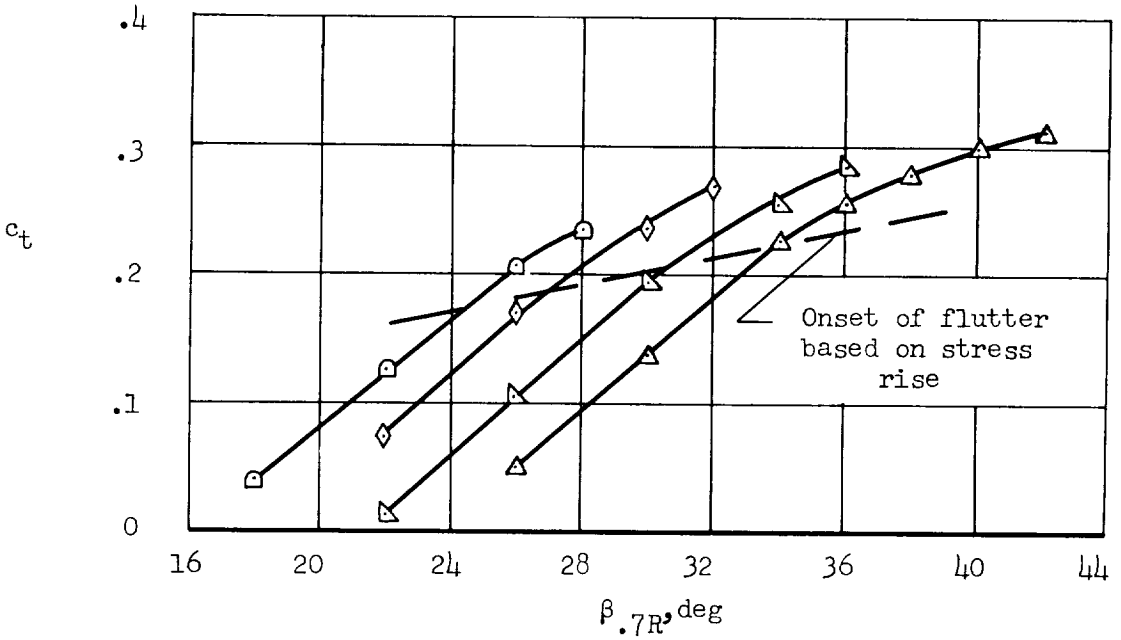

(b) Survey tube location; x = 0.78.

Figure 9.- Continued.

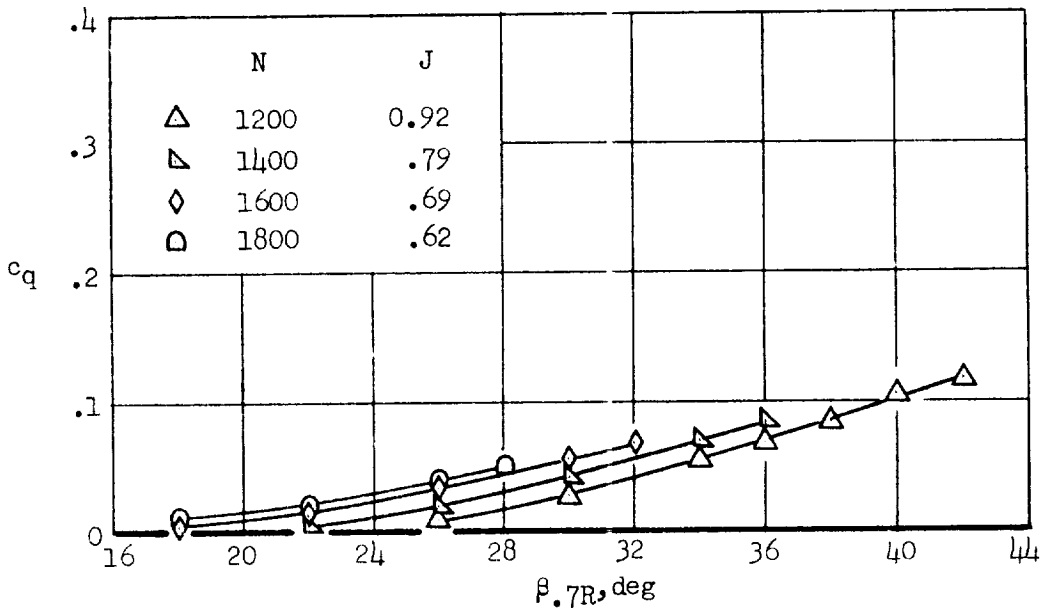

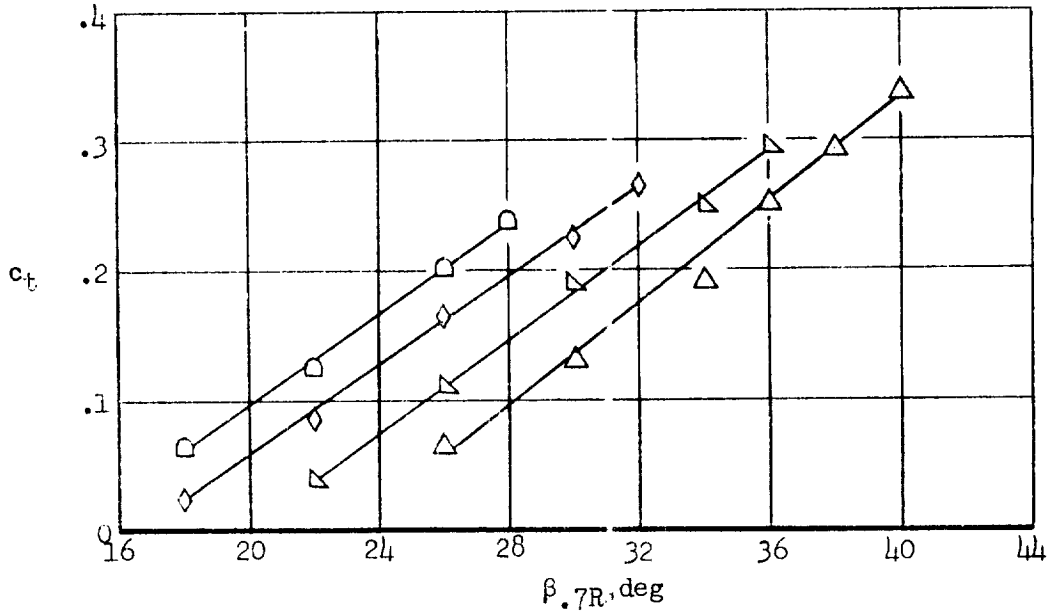

(c) Survey tube location; x = 0.64.

Figure 9.- Continued.

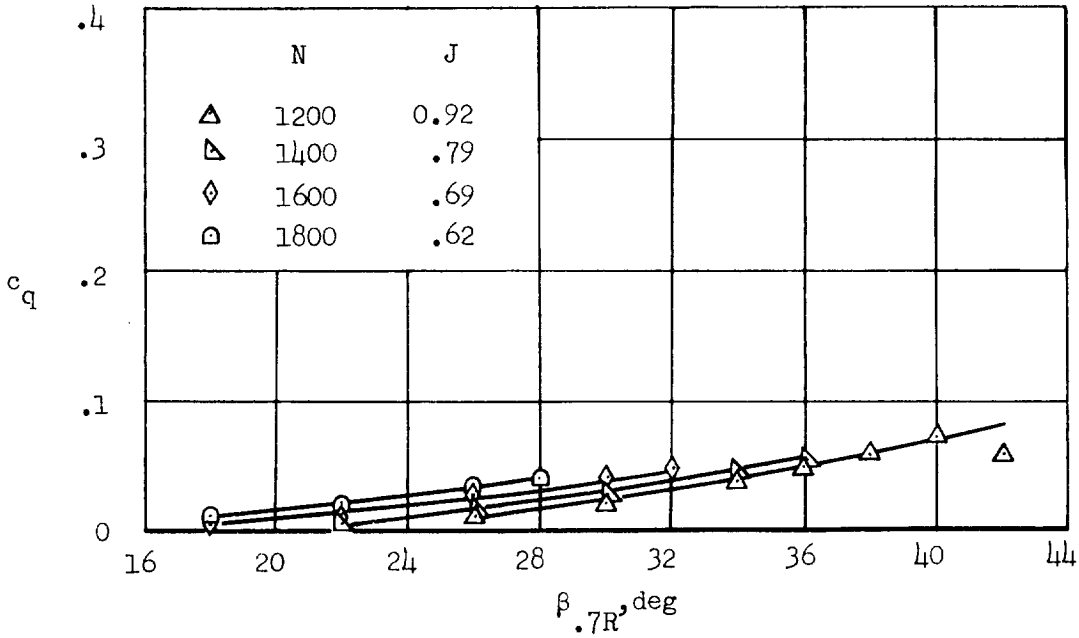

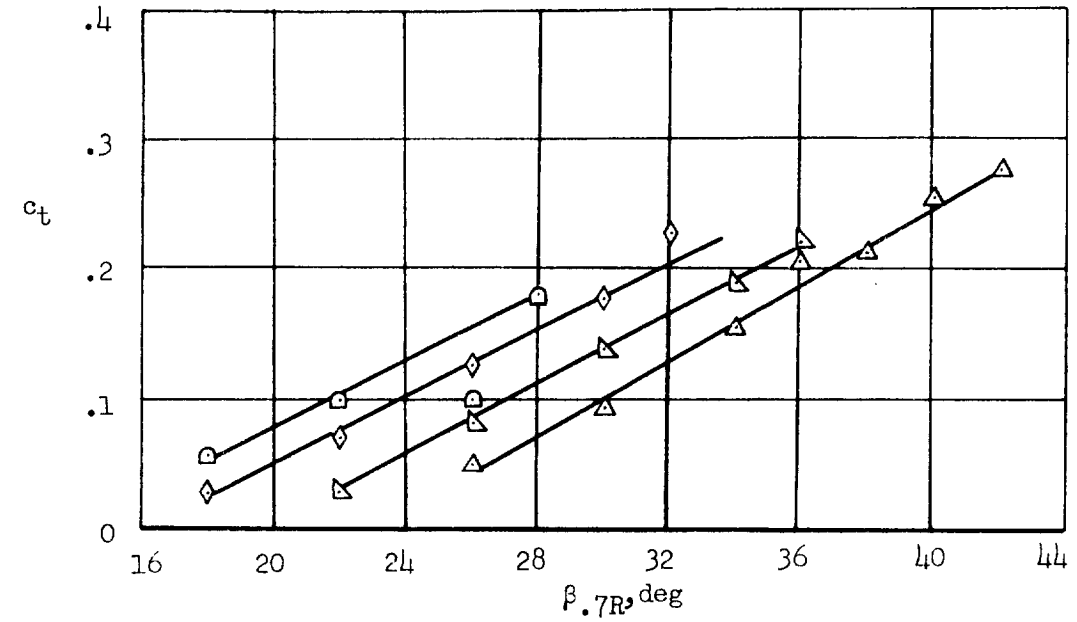

(d) Survey tube location; x = 0.50.

Figure 9.- Continued.

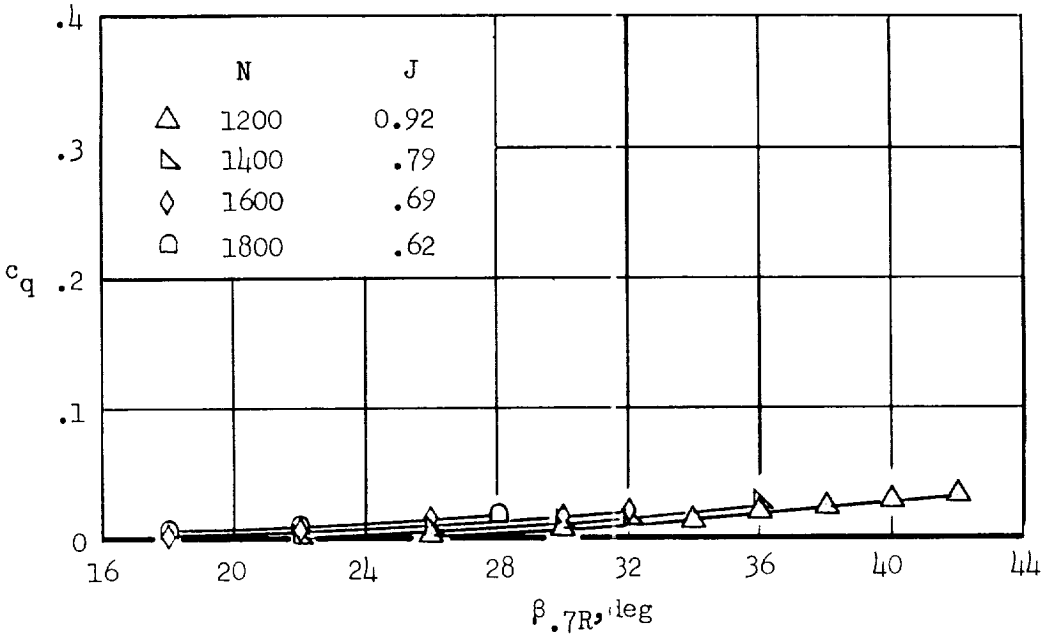

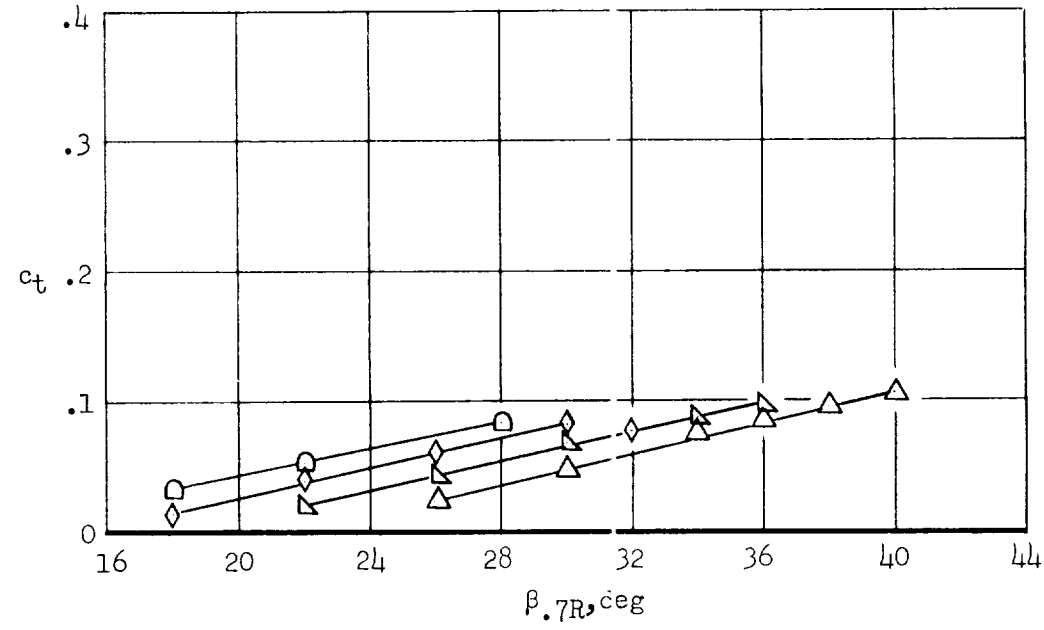

(e) Survey tube location; x = 0.37.

Figure 9.- Concluded.

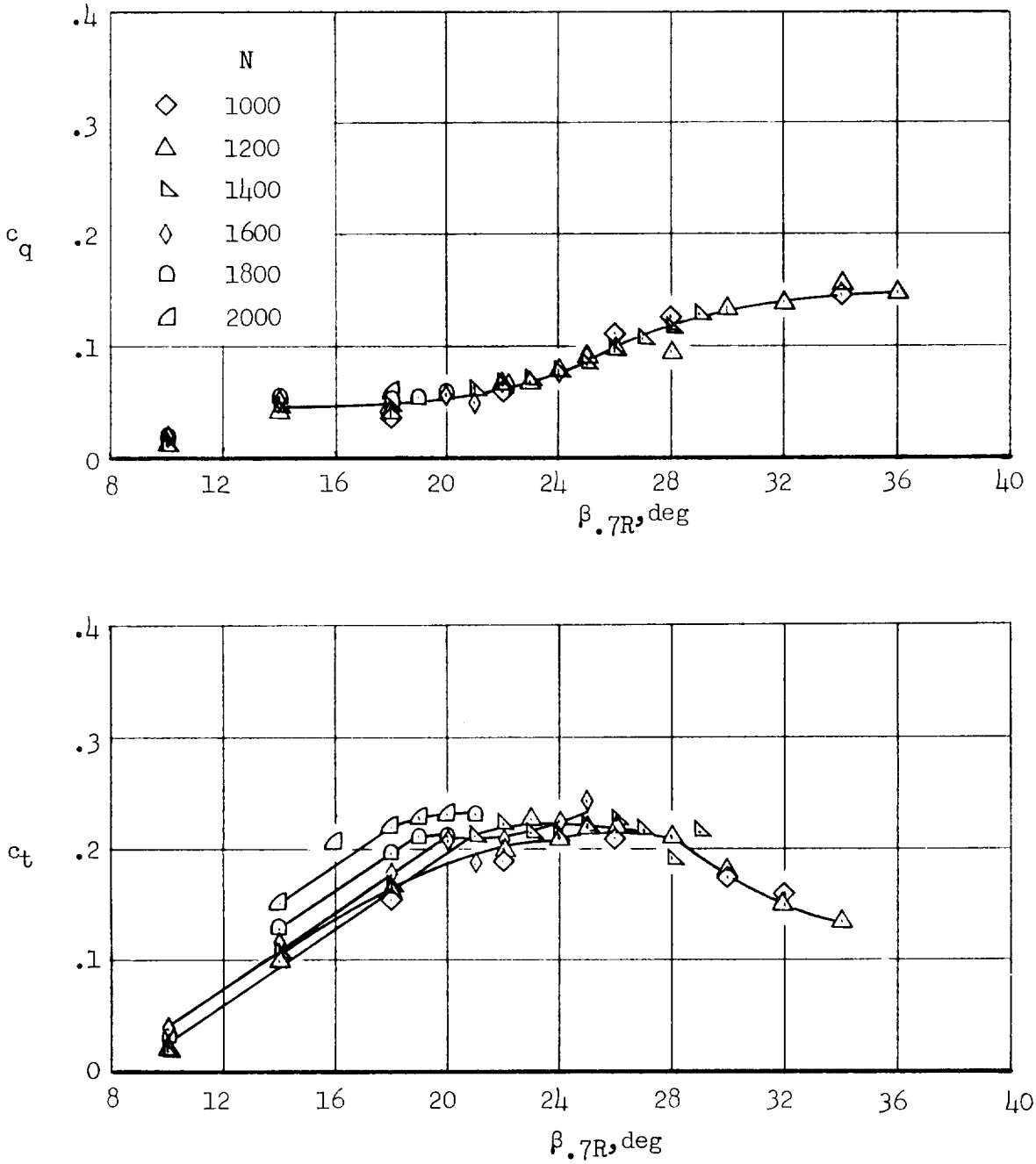

(a) Survey tube location; x = 0.78.

igure 10.- Variation of the measured section torque coefficient, c_q, and section thrust coefficient, c_t, with blade angle at $V_\infty \sim 0$; $\alpha_G = 10^\circ$.

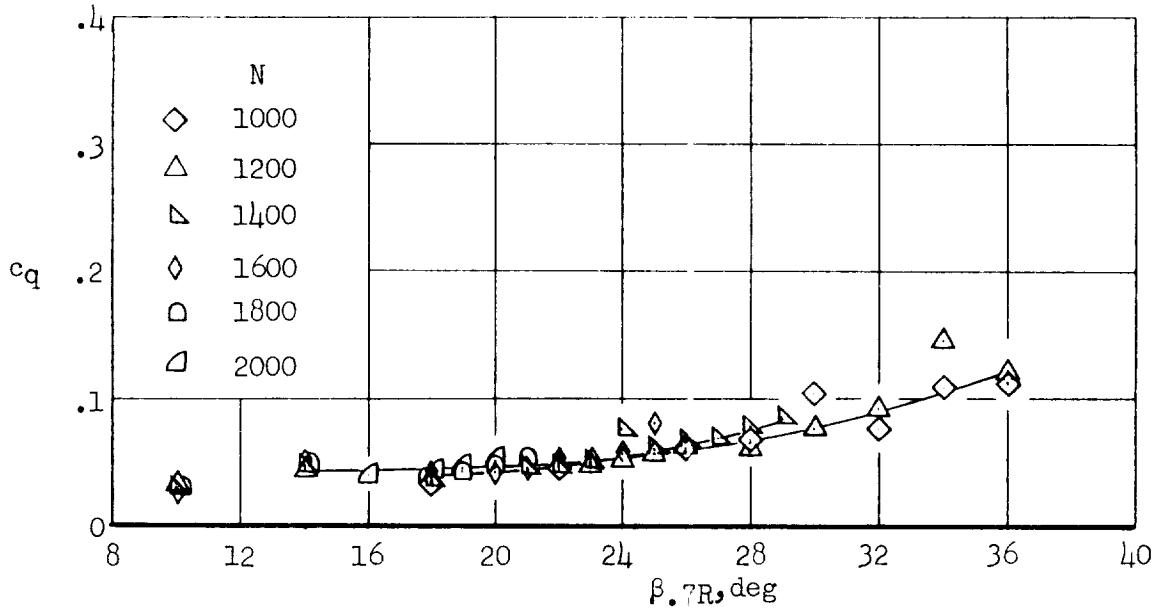

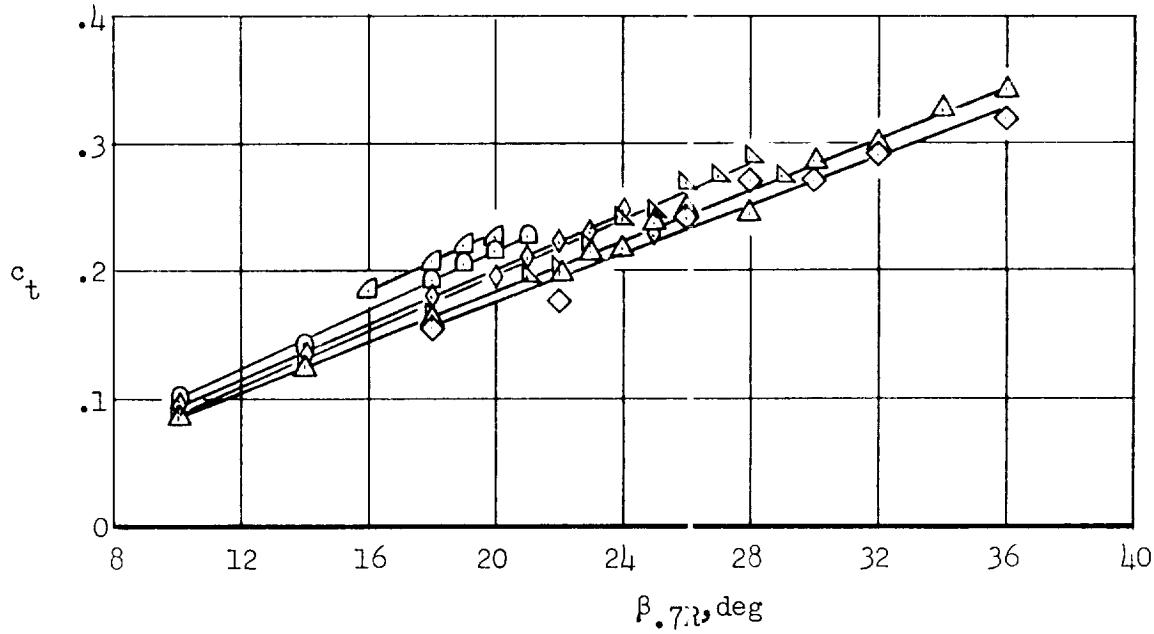

(b) Survey tube location; x = 0.64.

Figure 10.- Concluded.

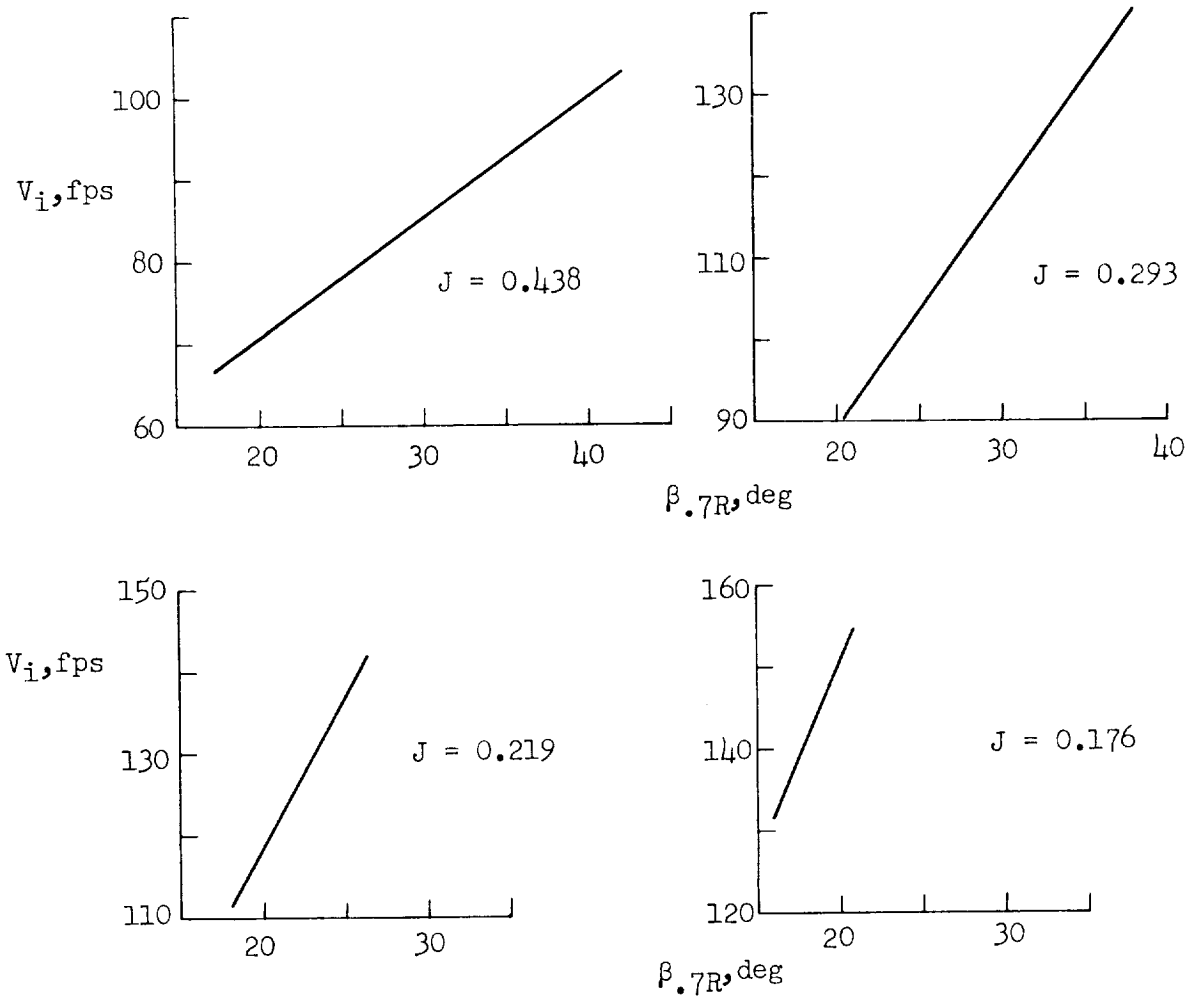

(a) V_∞ = 58.5 fps; x = 0.38

Figure 11.- Variation of the measured inflow velocity, V_i, with blade angle for several values of advance ratio, J; $\alpha_G = 0^o$.

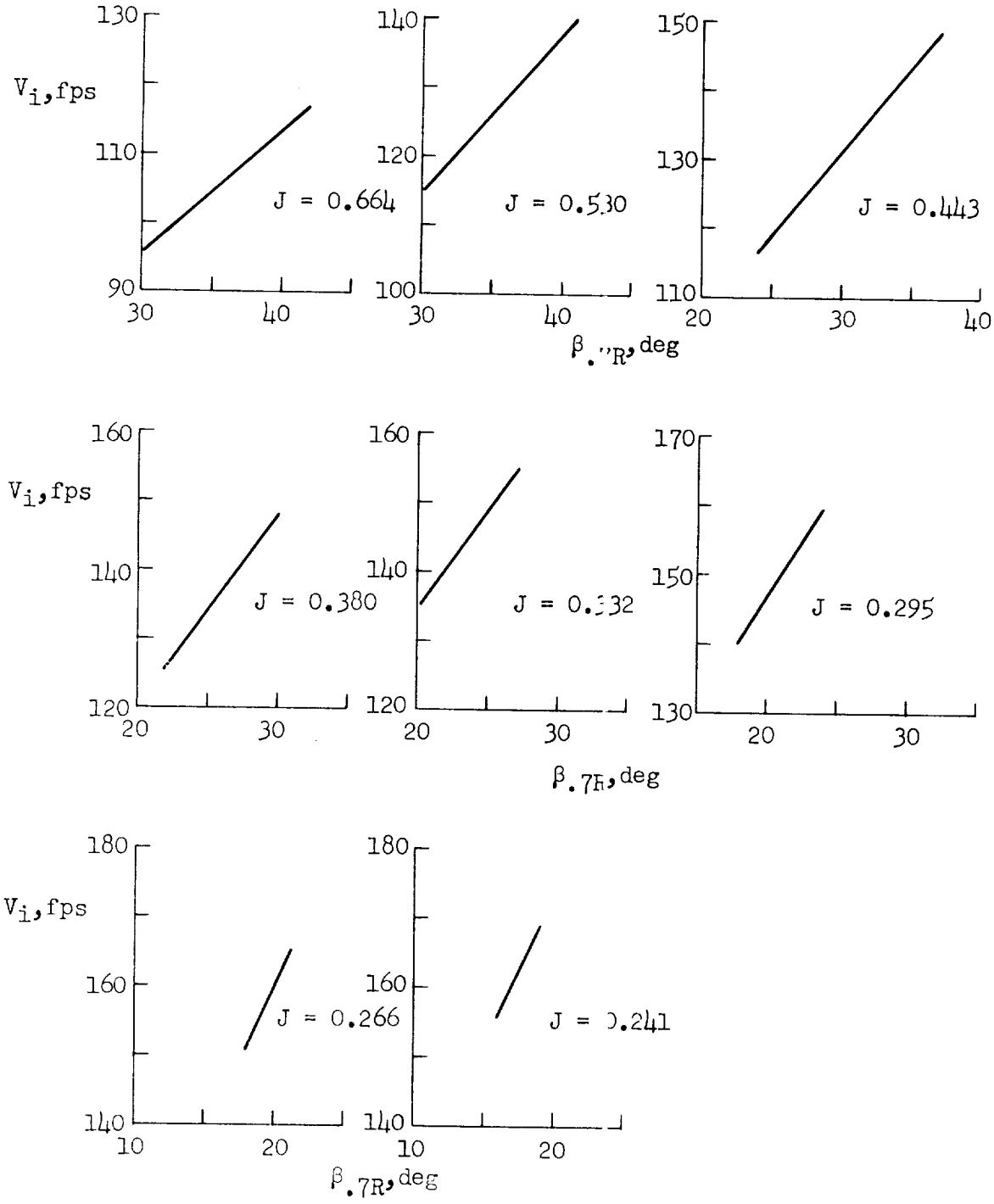

(b) V_∞ = 88.5 fps; x = 0.38

Figure 11.- Continued.

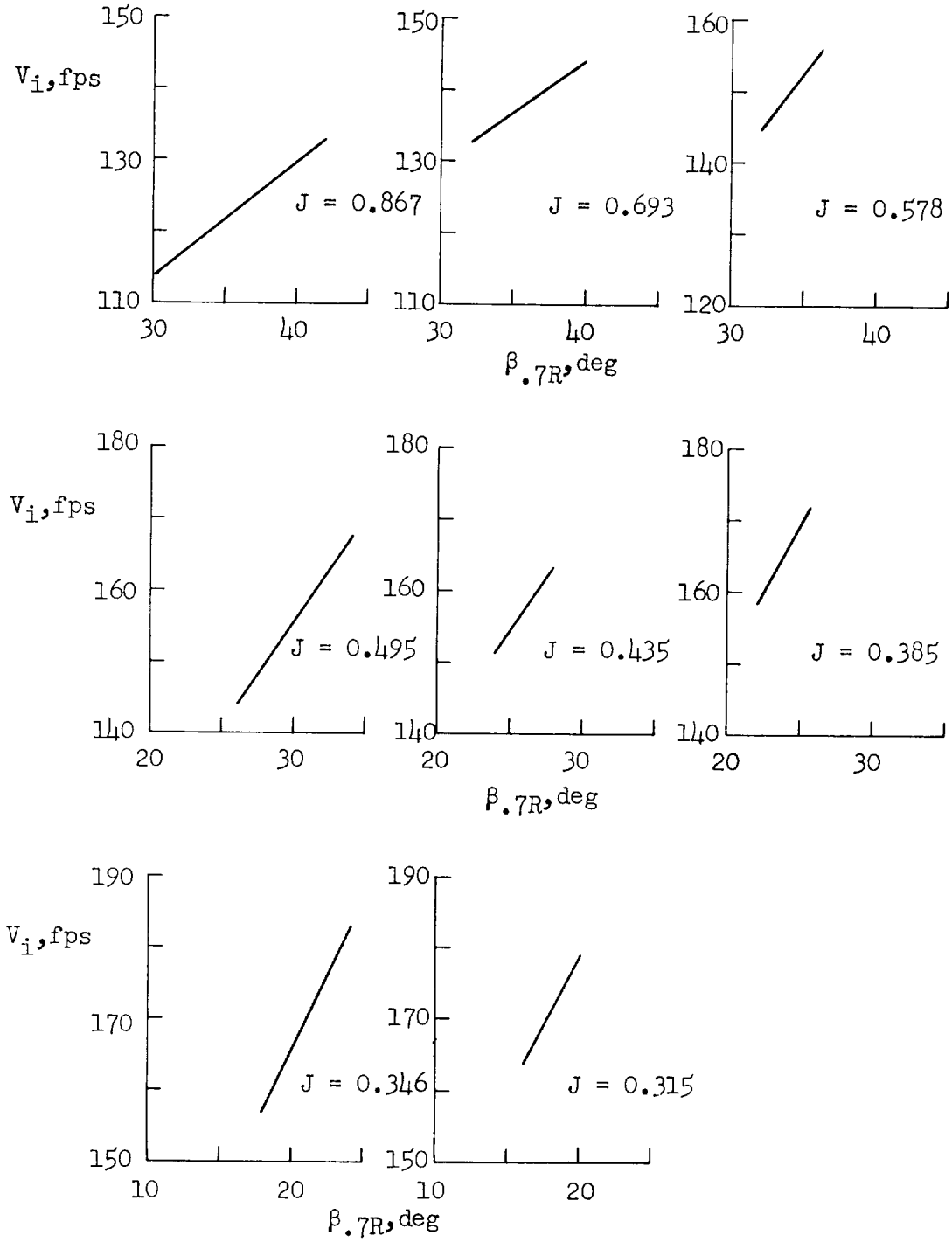

(c) V_∞ = 115.5 fps; x = 0.38

Figure 11.- Continued.

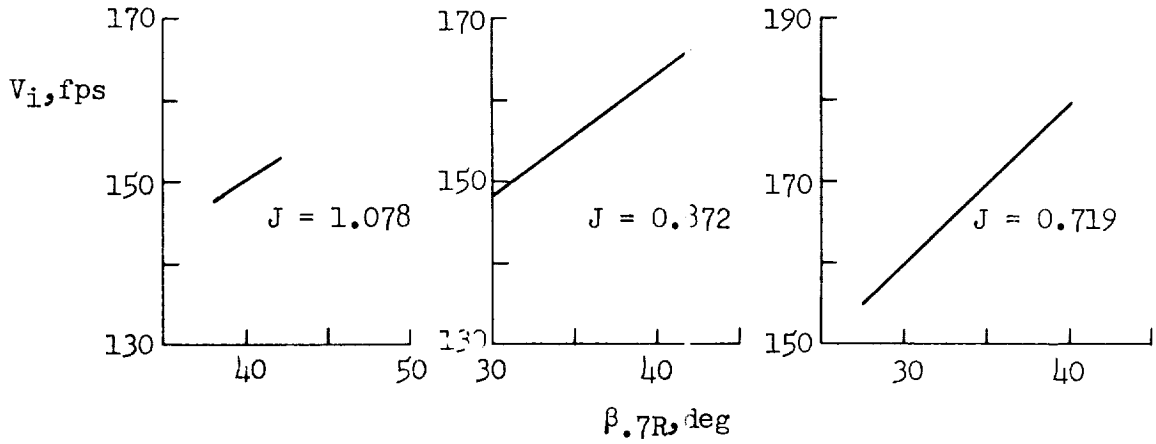

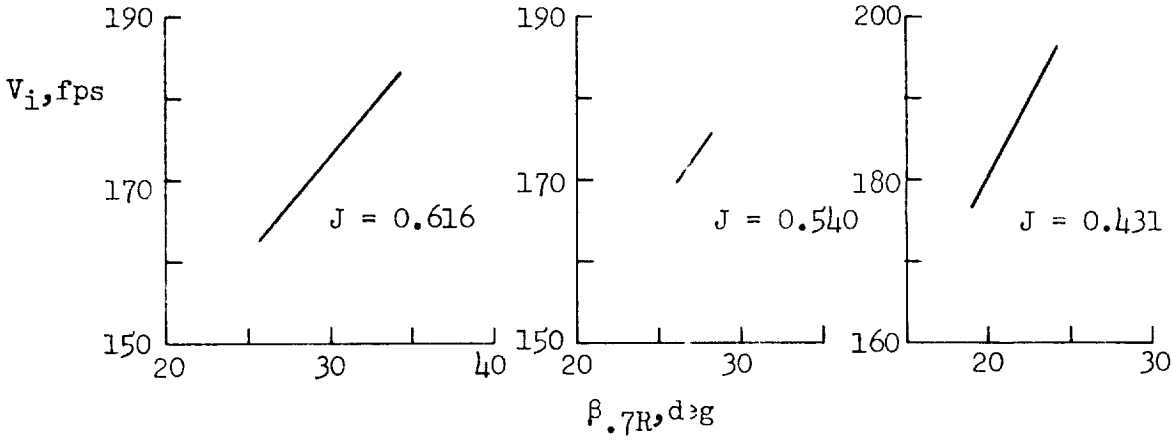

(d) V_∞ = 143.8 fps: x = 0.38

Figure 11.- Continued.

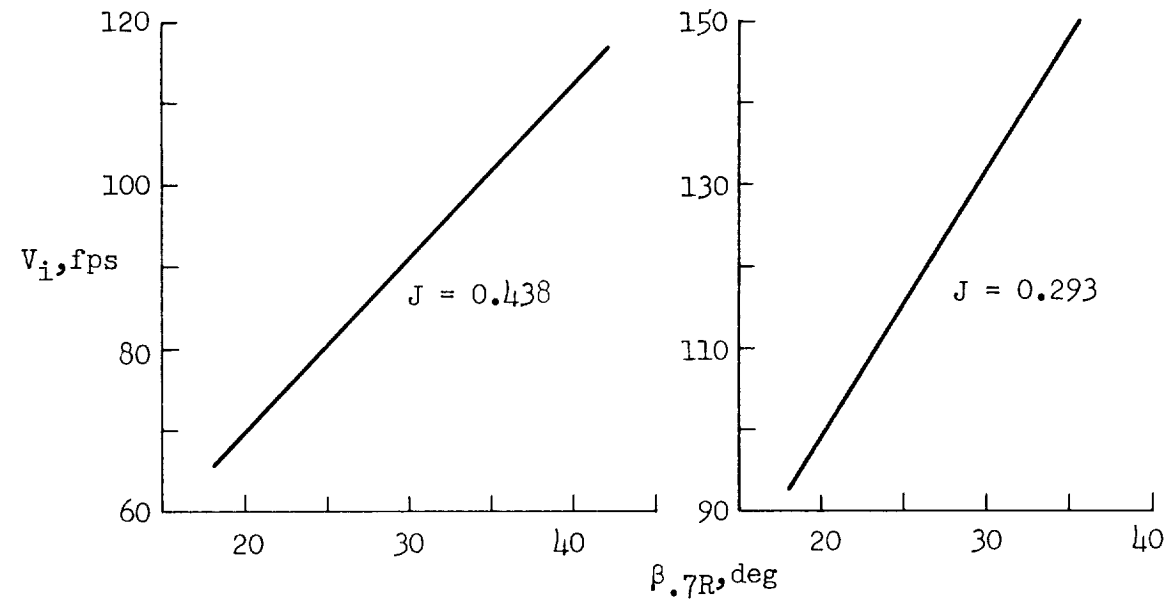

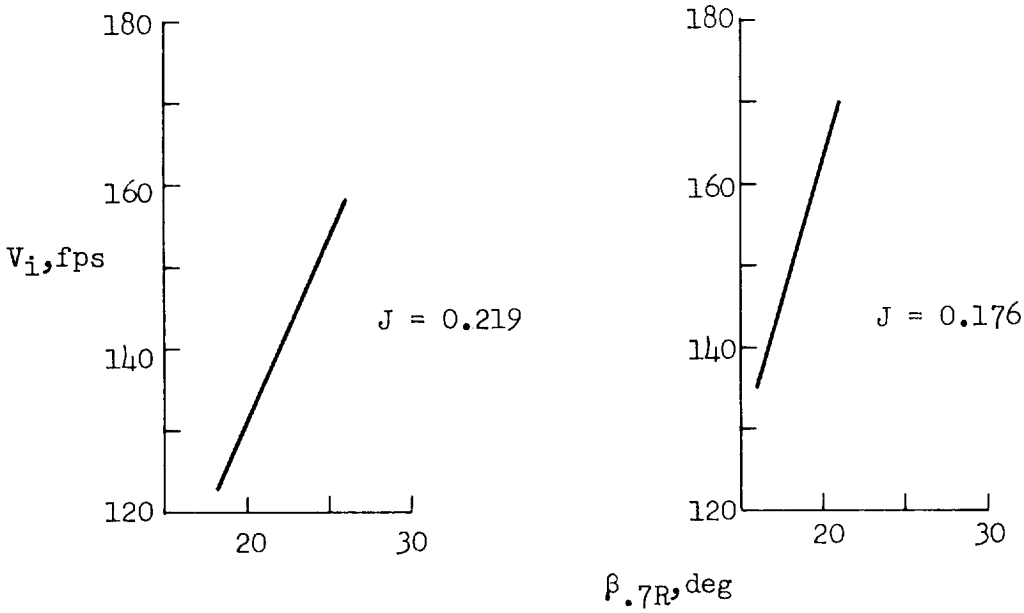

(e) V_∞ = 58.5 fps; x = 0.58

Figure 11.- Continued.

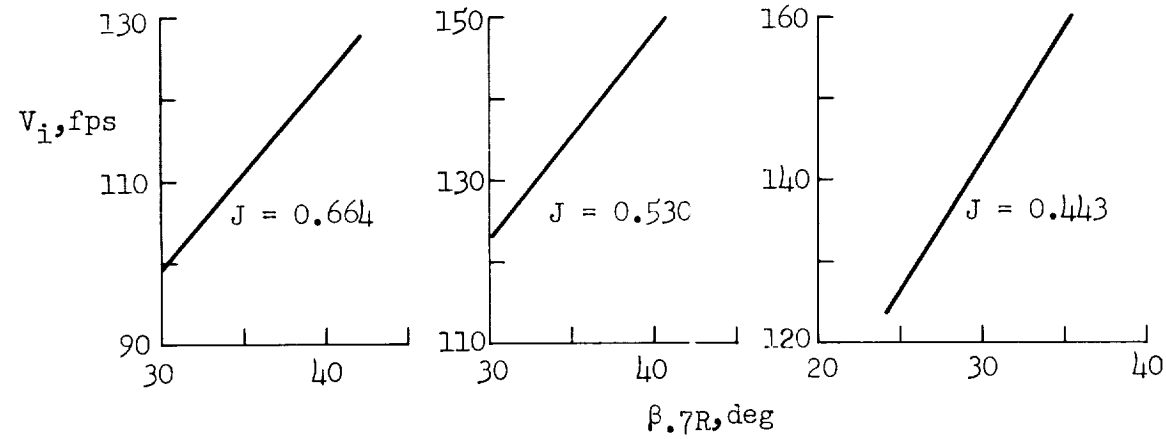

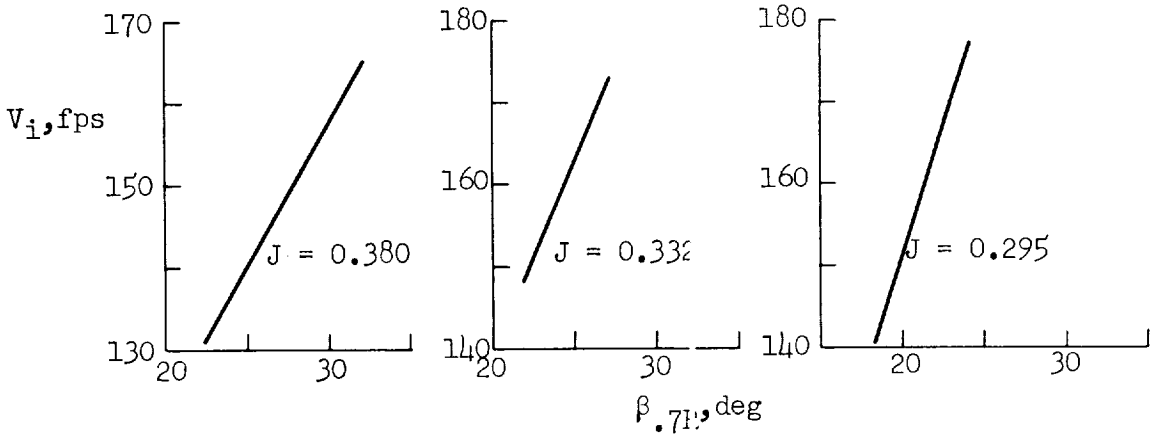

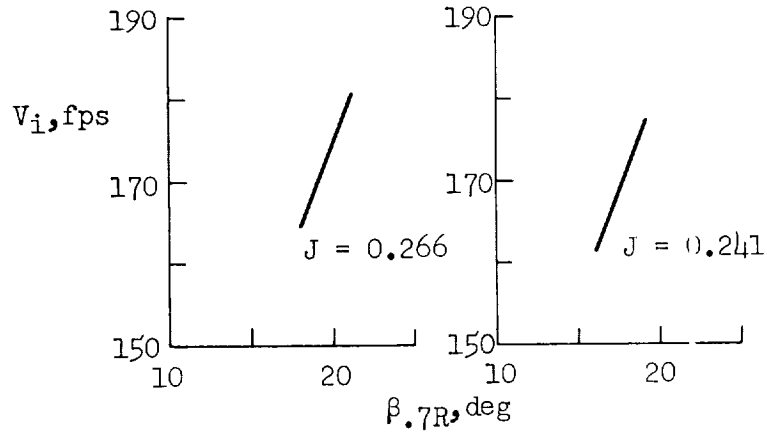

(f) V_∞ = 88.5 fps; x = 0.58

Figure 11.- Continued.

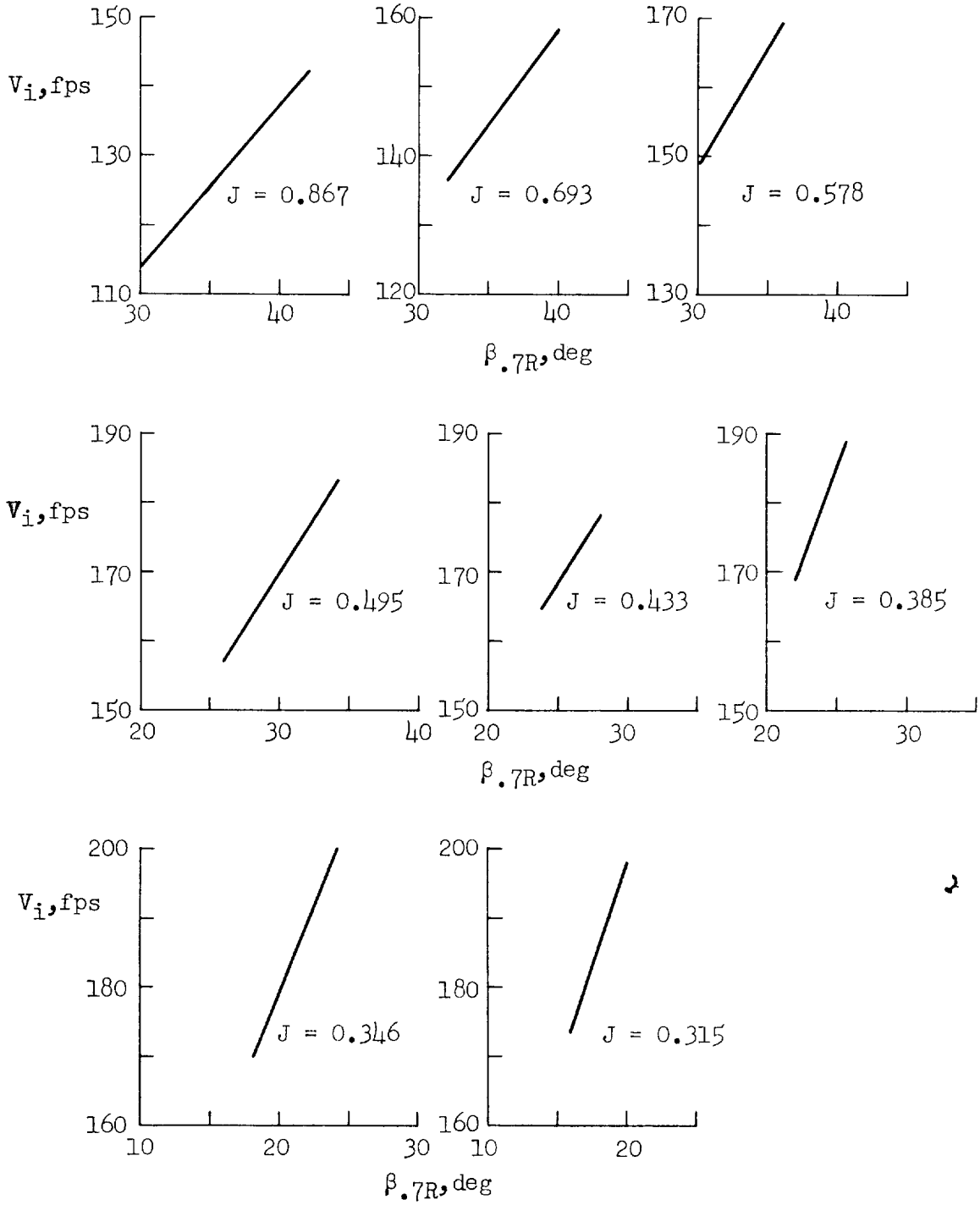

(g) V_∞ = 115.5 fps; x = 0.58

Figure 11.- Continued.

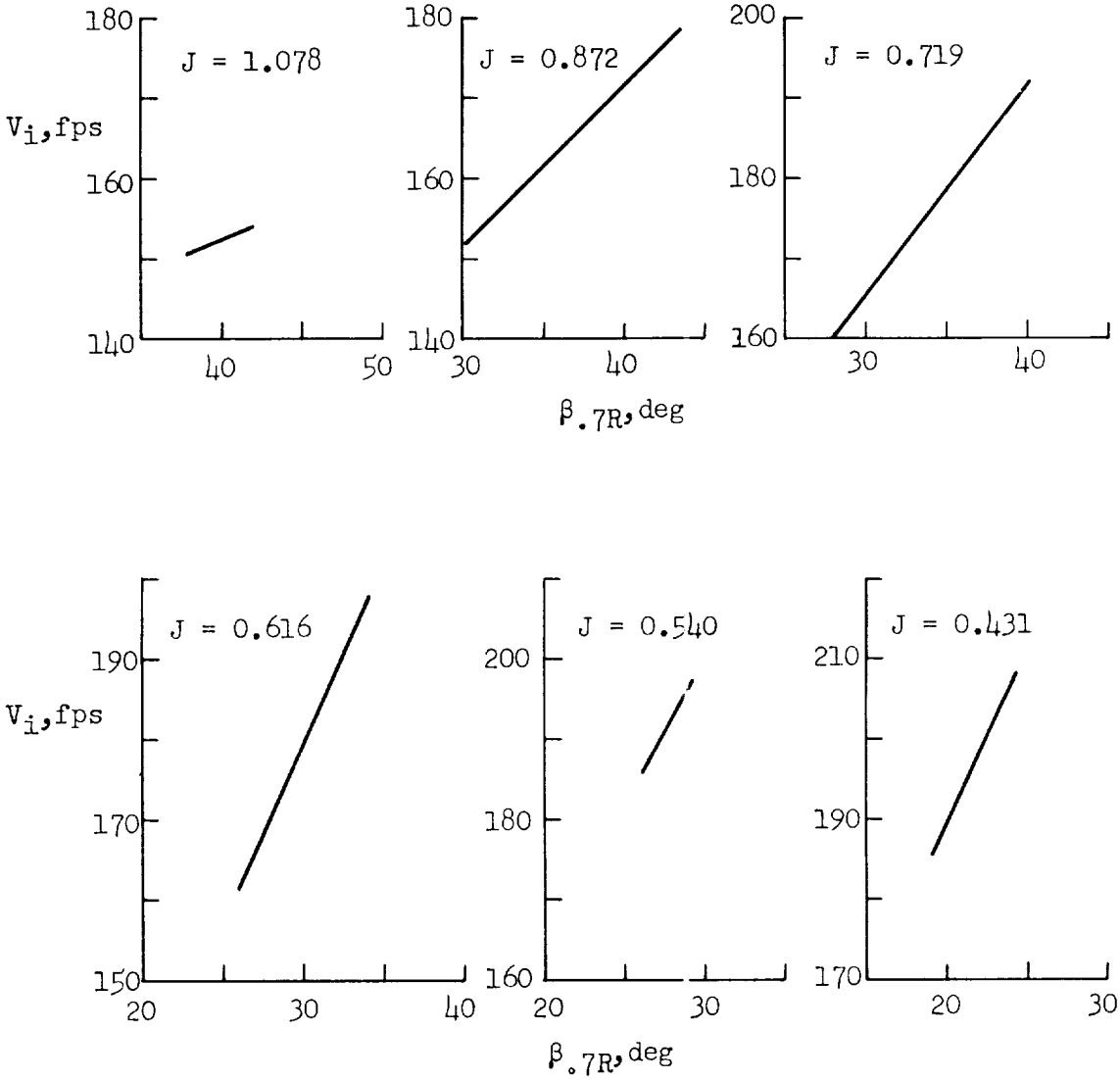

(h) V_∞ = 143.8 fps; x = 0.58

Figure 11.- Continued.

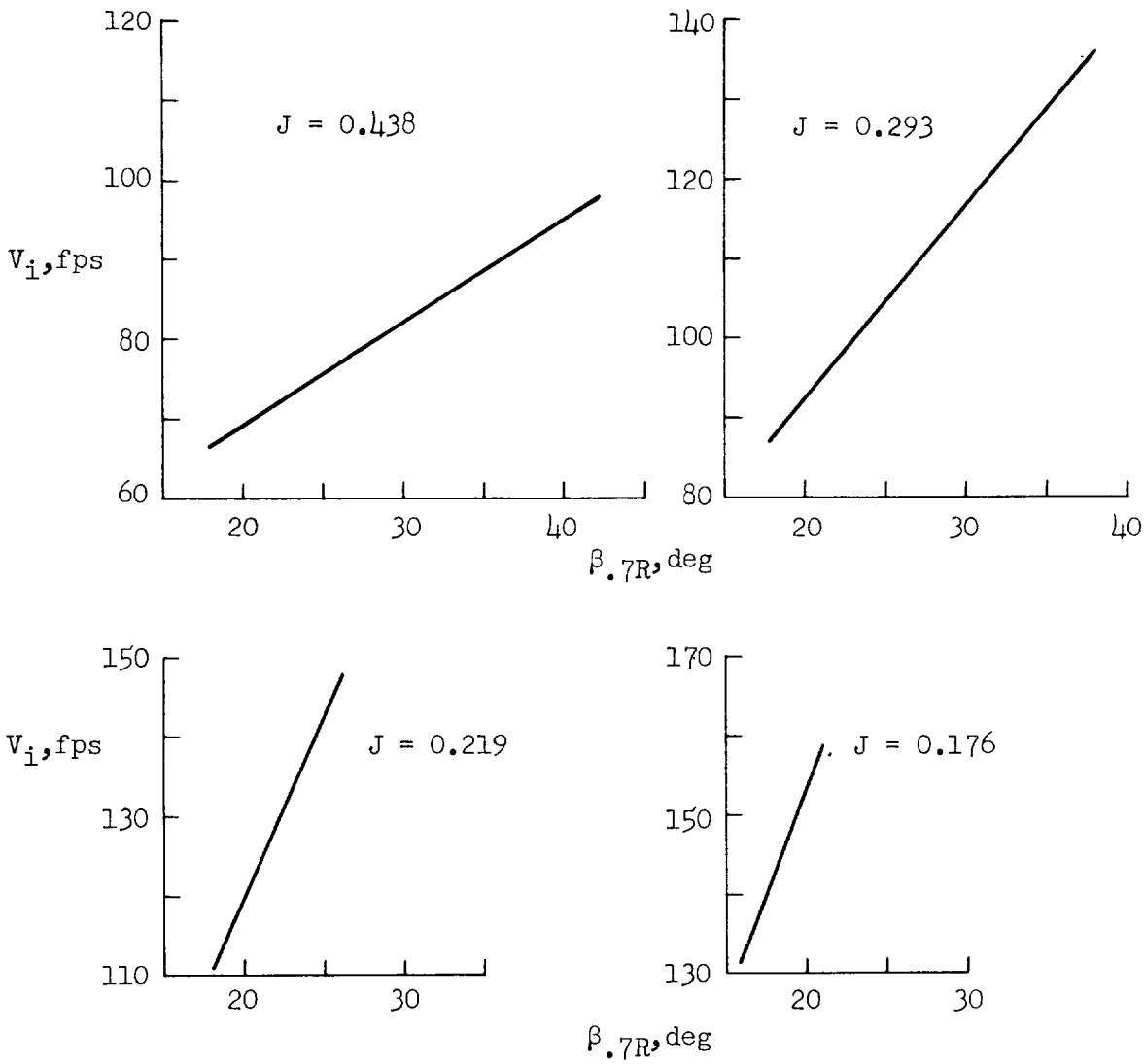

(i) V_∞ = 58.5 fps; x = 0.78

Figure 11.- Continued.

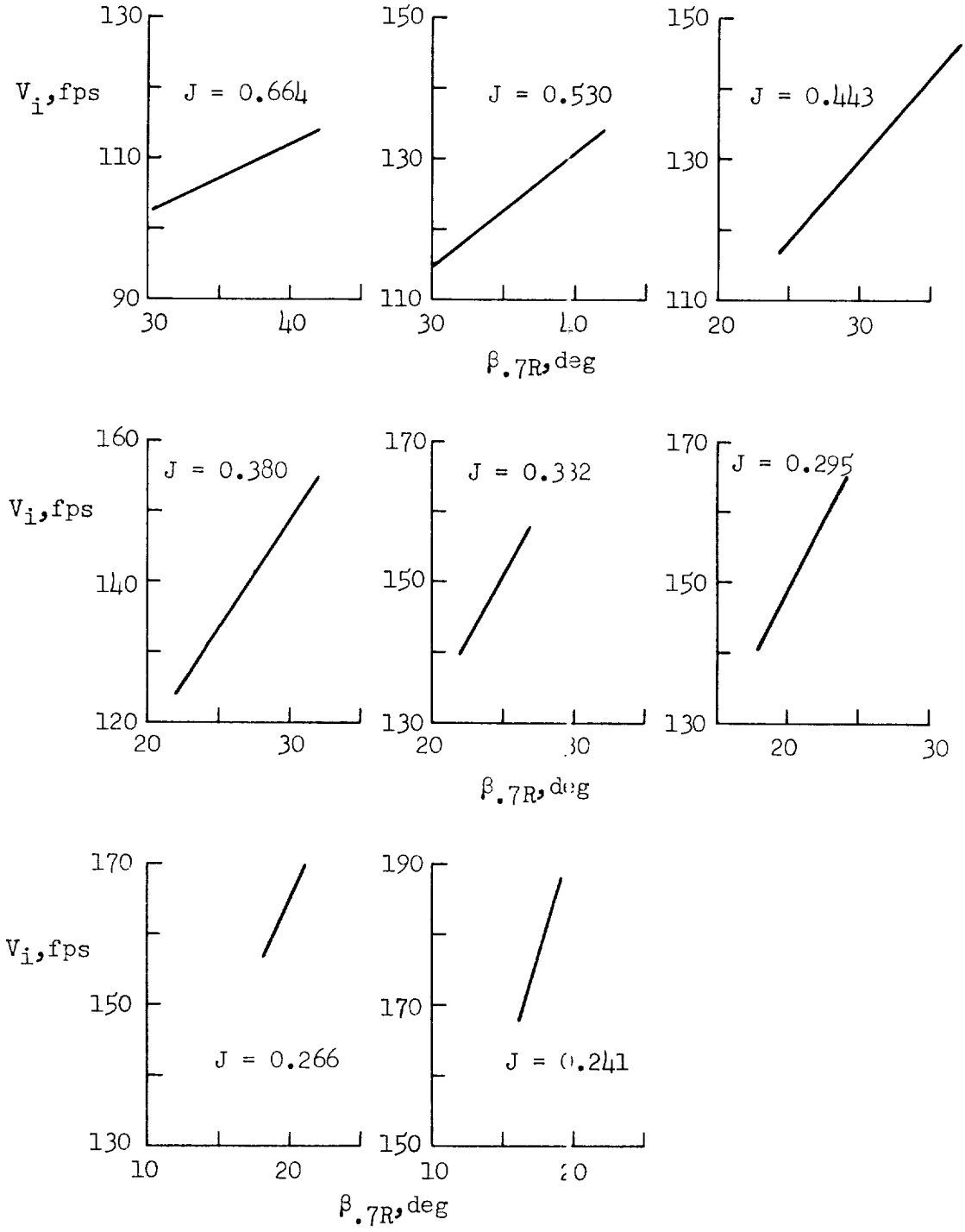

(j) V_∞ = 88.5 fps; μ = 0.78

Figure 11.- Continued.

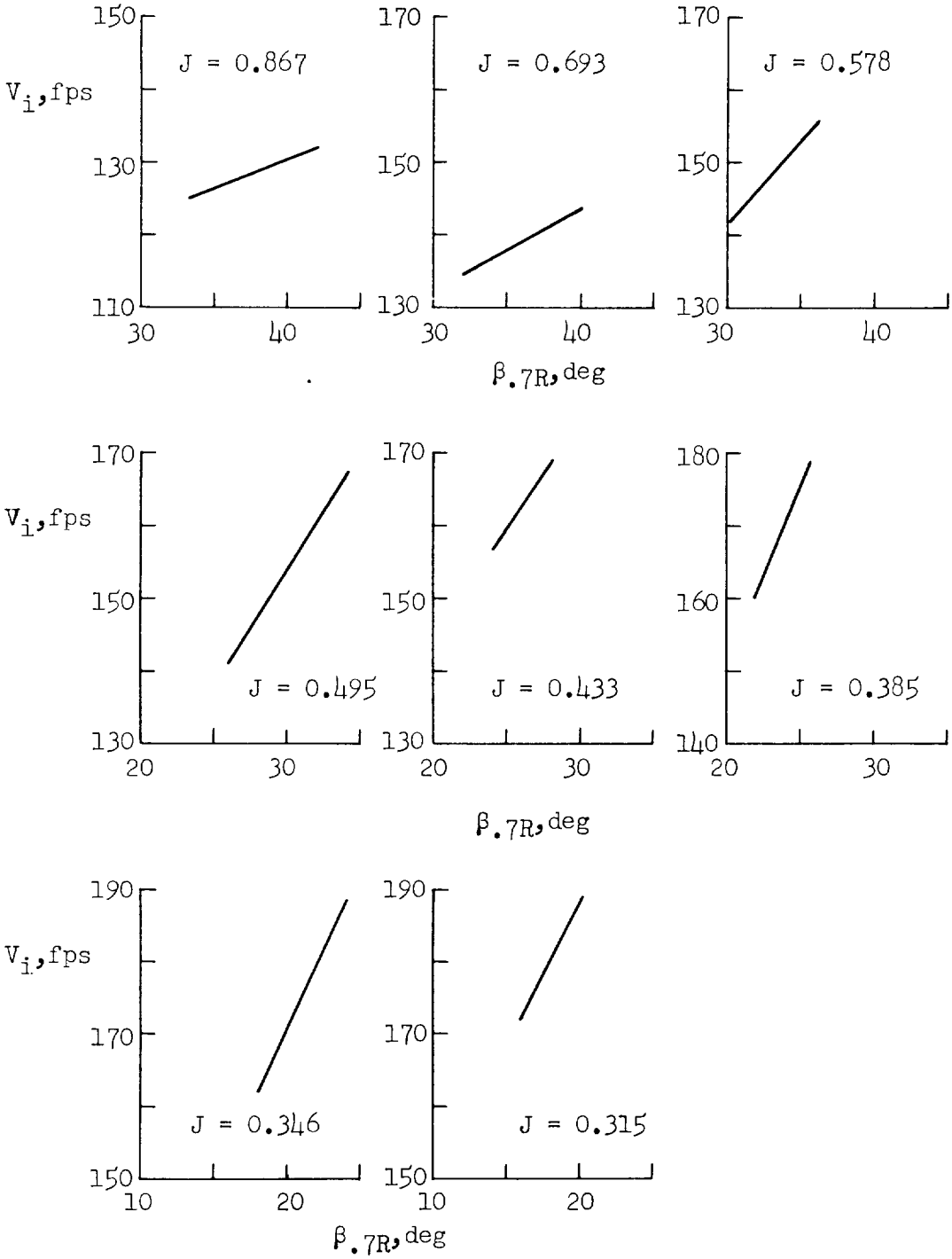

(k) V_∞ = 115.5 fps; x = 0.78

Figure 11.- Continued.

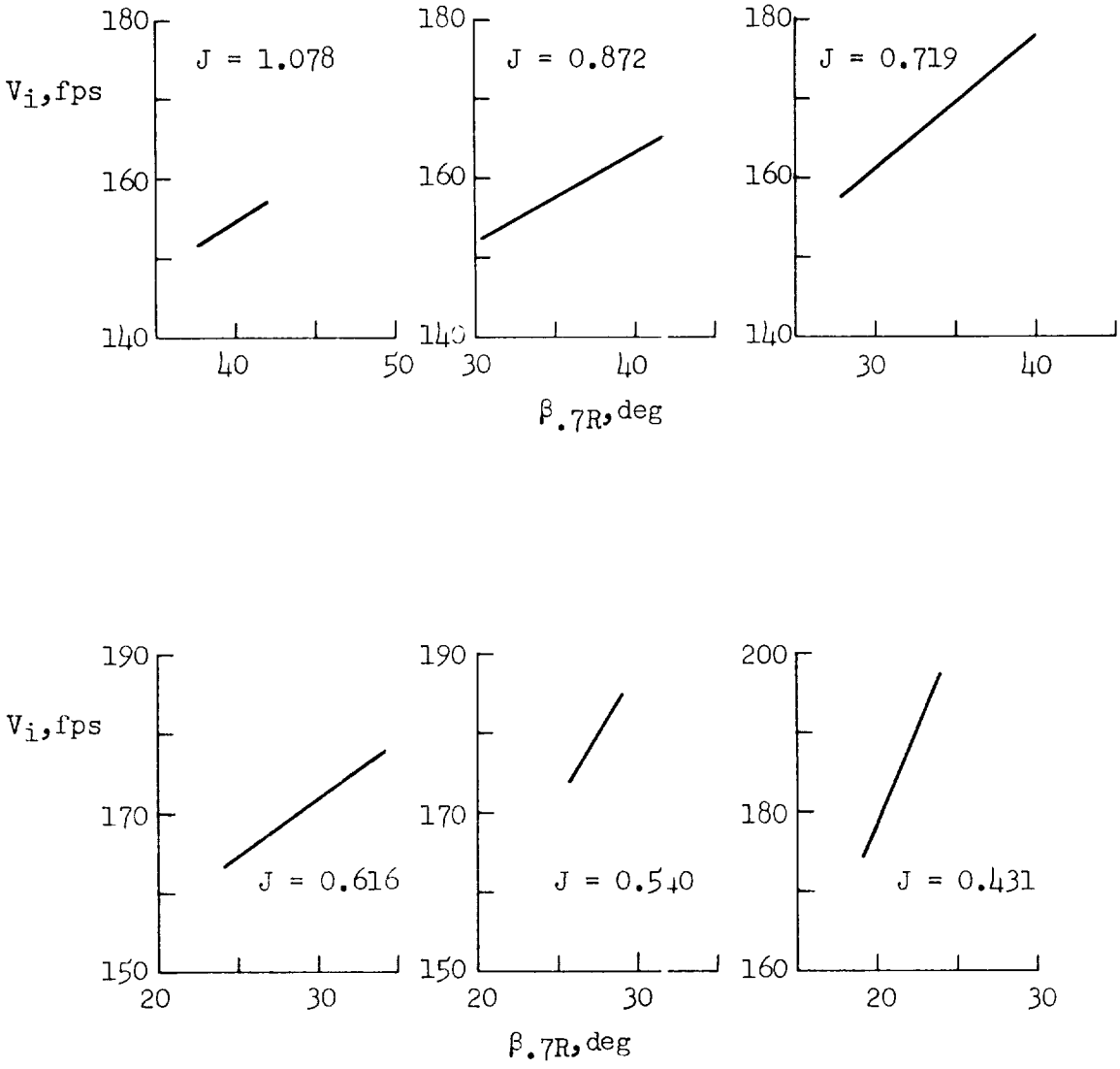

(l) V_∞ = 143.8 fps; x = 0.78

Figure 11.- Concluded.

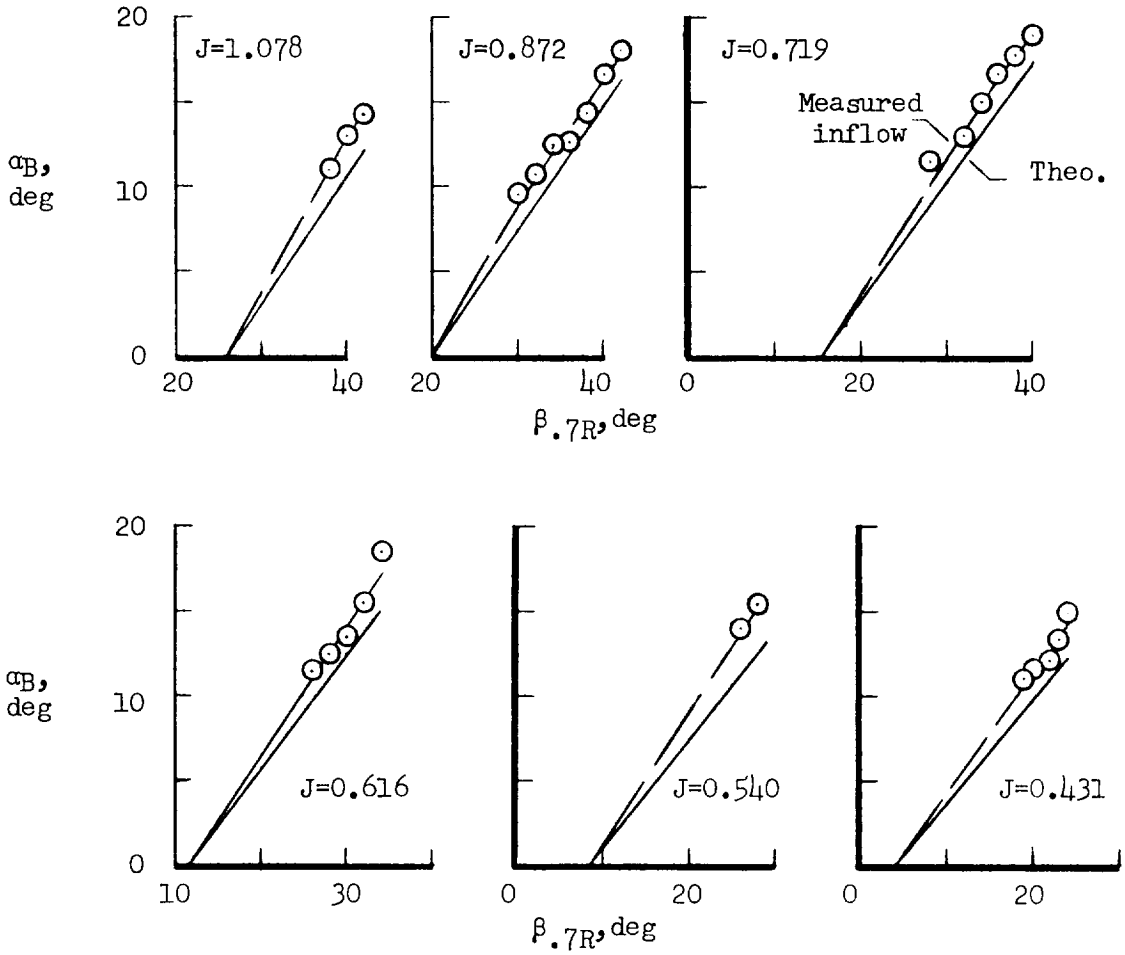

(a) V_∞ = 143.8 fps; x = 0.38

Figure 12.- Comparison of the computed variation of local blade-section angle of attack with that obtained by use of measured inflow velocities as a function of blade angle for several values of advance ratio; $\alpha_G = 0^\circ$.

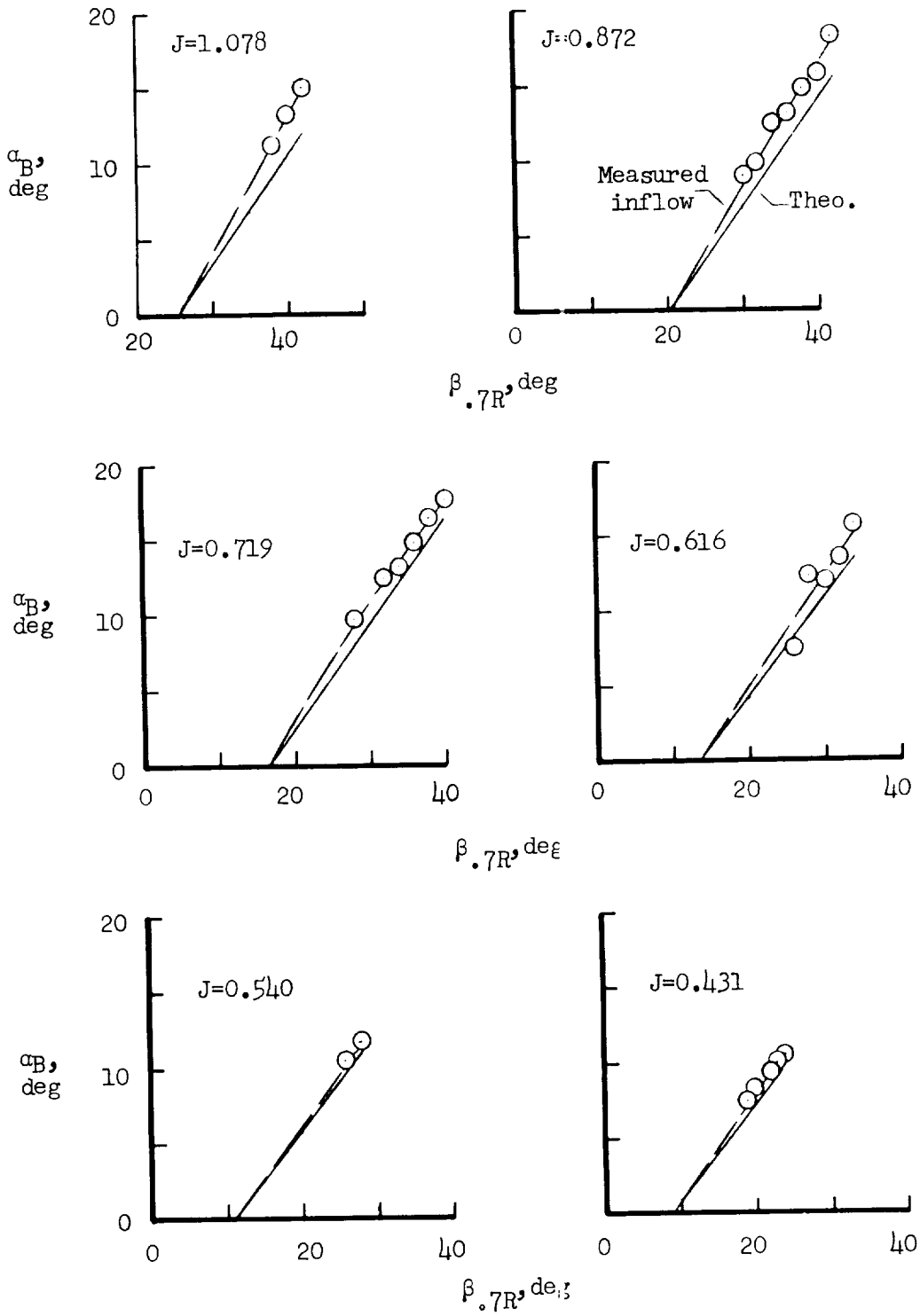

(b) V_∞ = 143.8 fps; x = 0.58

Figure 12.- Continued.

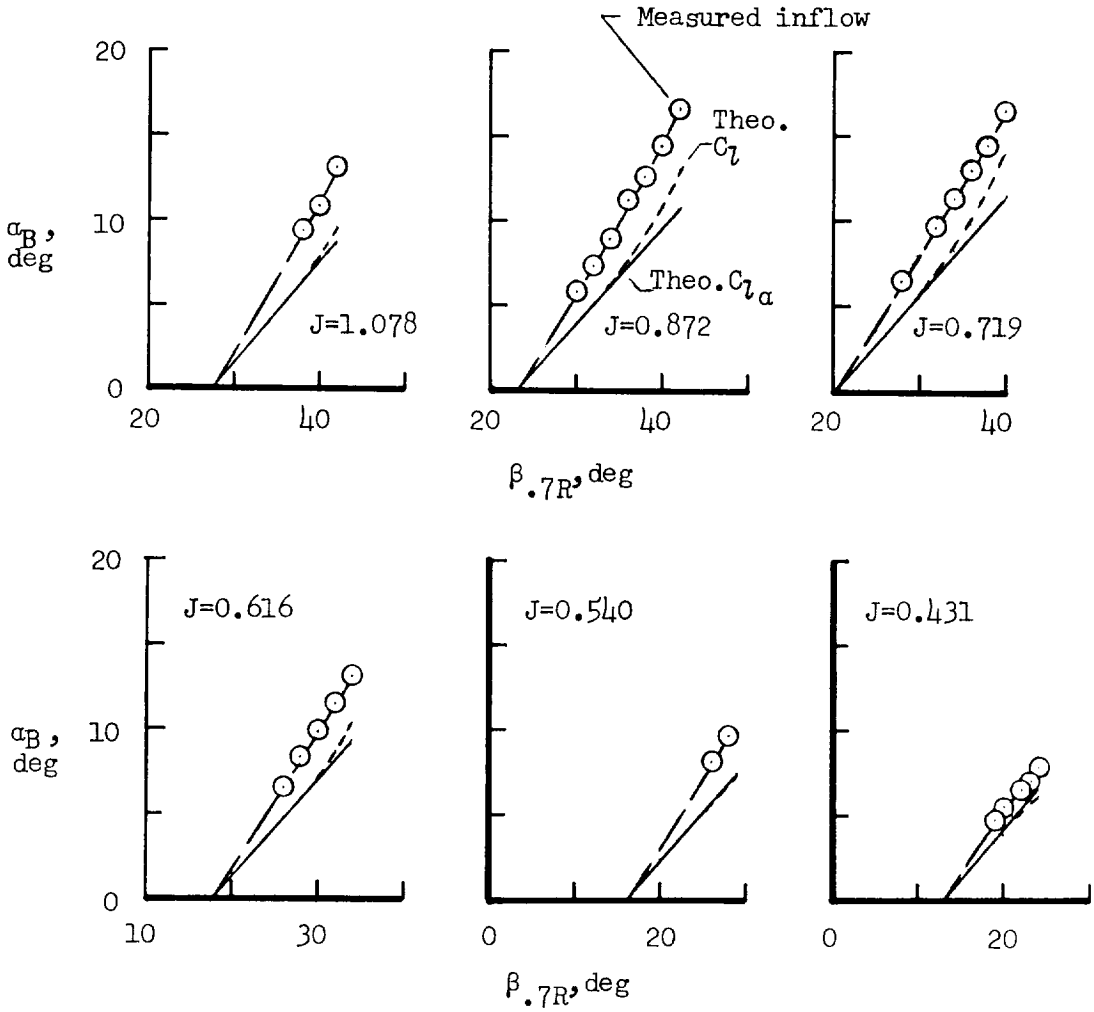

(c) V_∞ = 143.8 fps; x = 0.78

Figure 12.- Concluded.

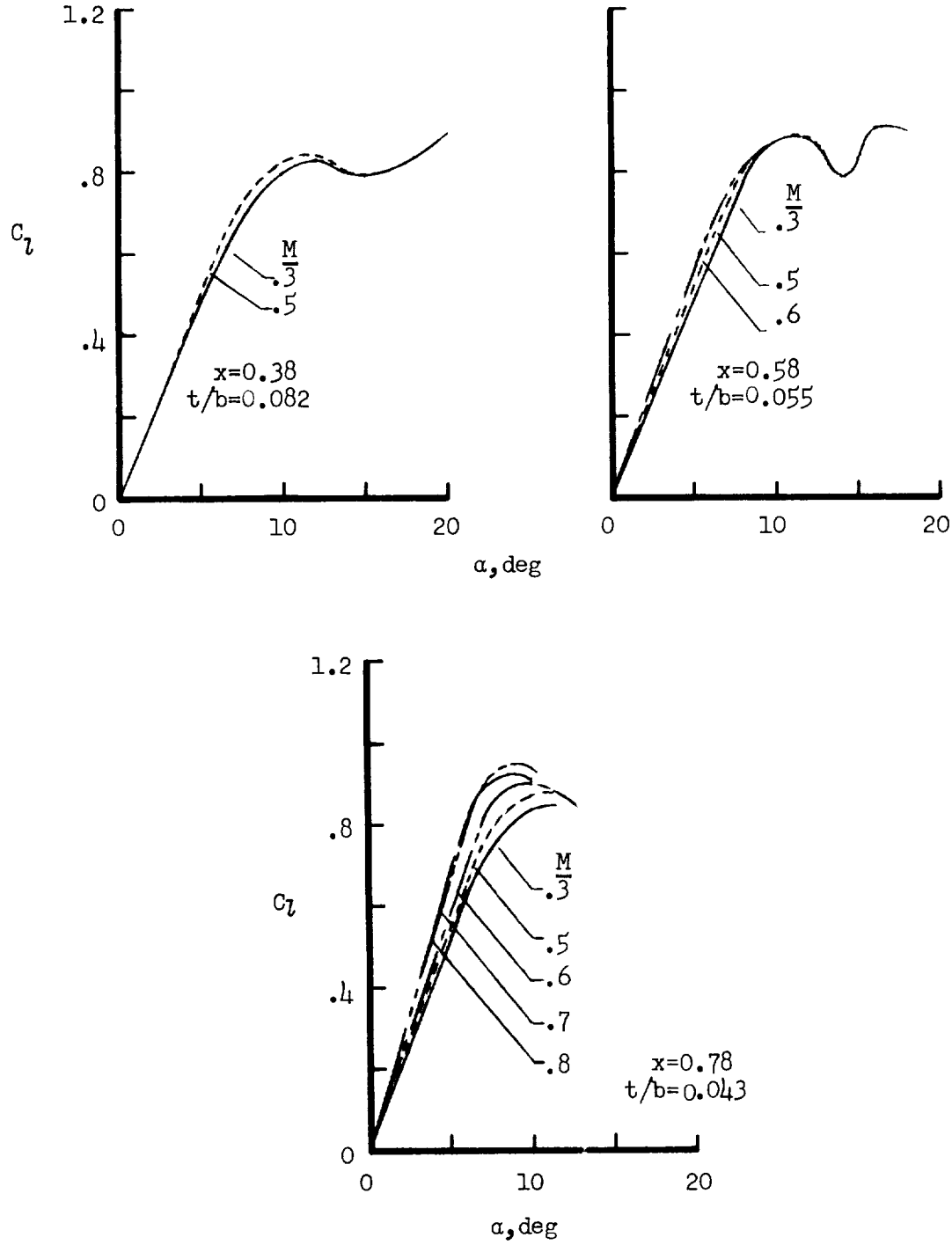

(a) Lift characteristics.

Figure 13.- Aerodynamic characteristics of symmetrical 16-series airfoil sections for several Mach numbers.

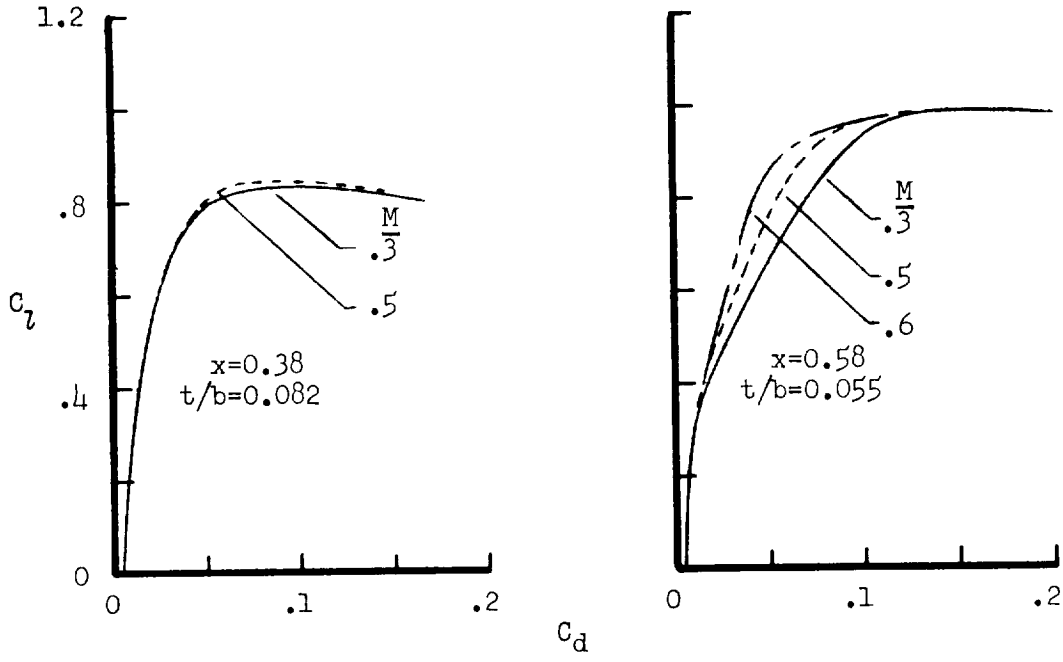

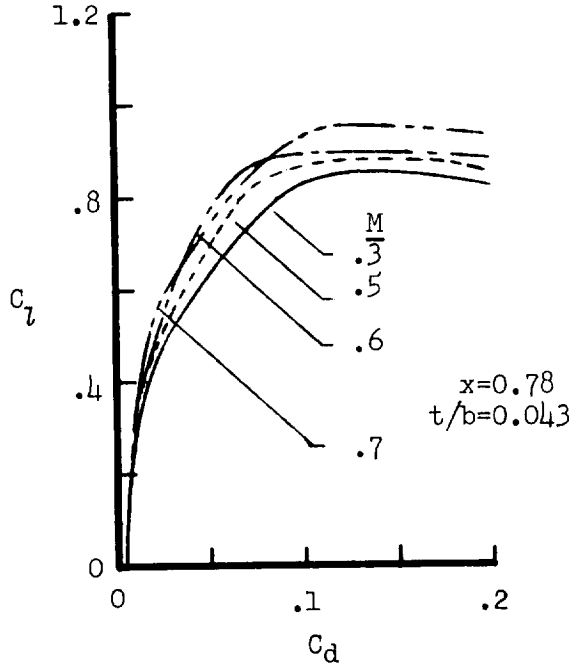

(b) Drag characteristics.

Figure 13.- Concluded.

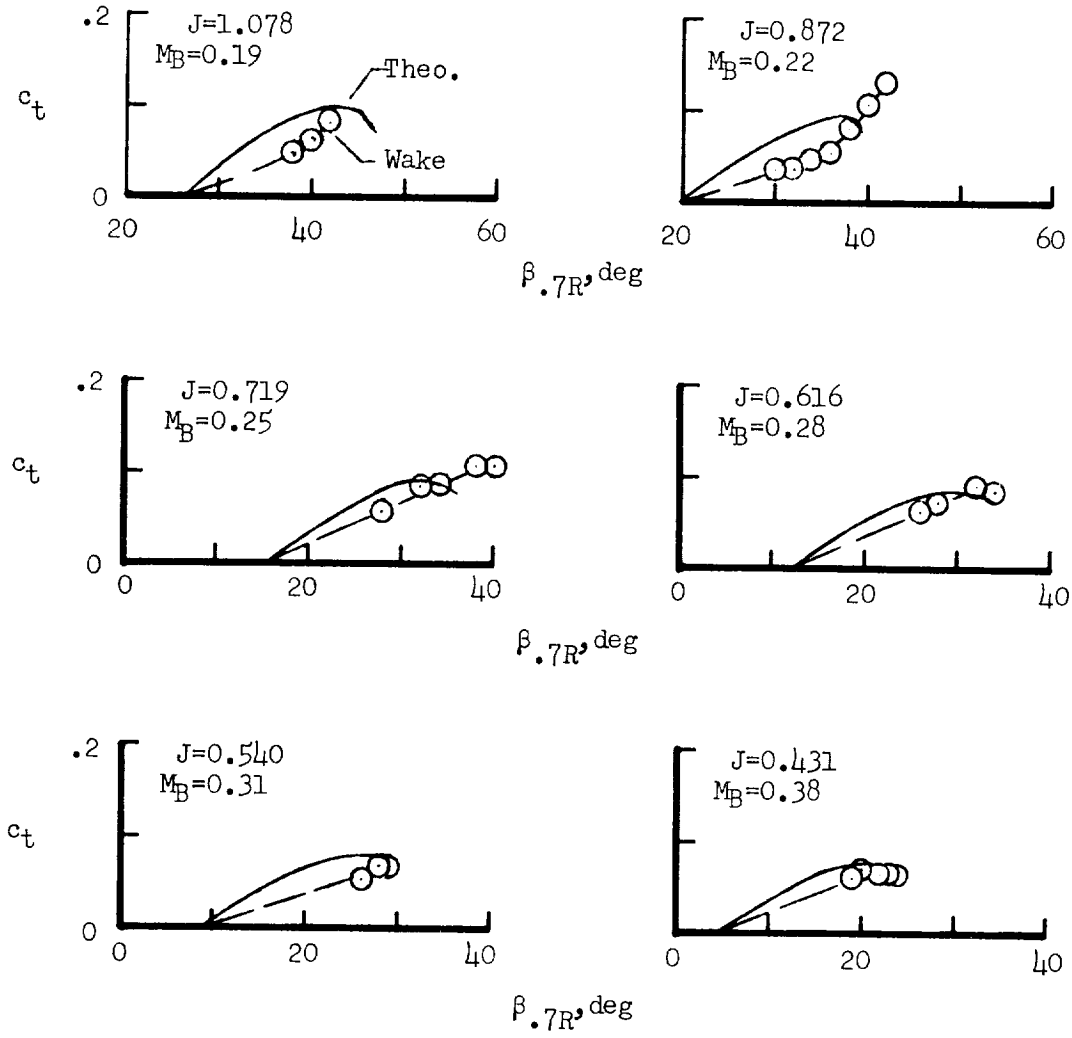

(a) V_∞ = 143.8 fps; x = 0.38

Figure 14.- Comparison of the computed and wake measured variation of the section thrust coefficient as a function of the propeller blade angle for several values of advance ratio; $\alpha_G = 0^\circ$.

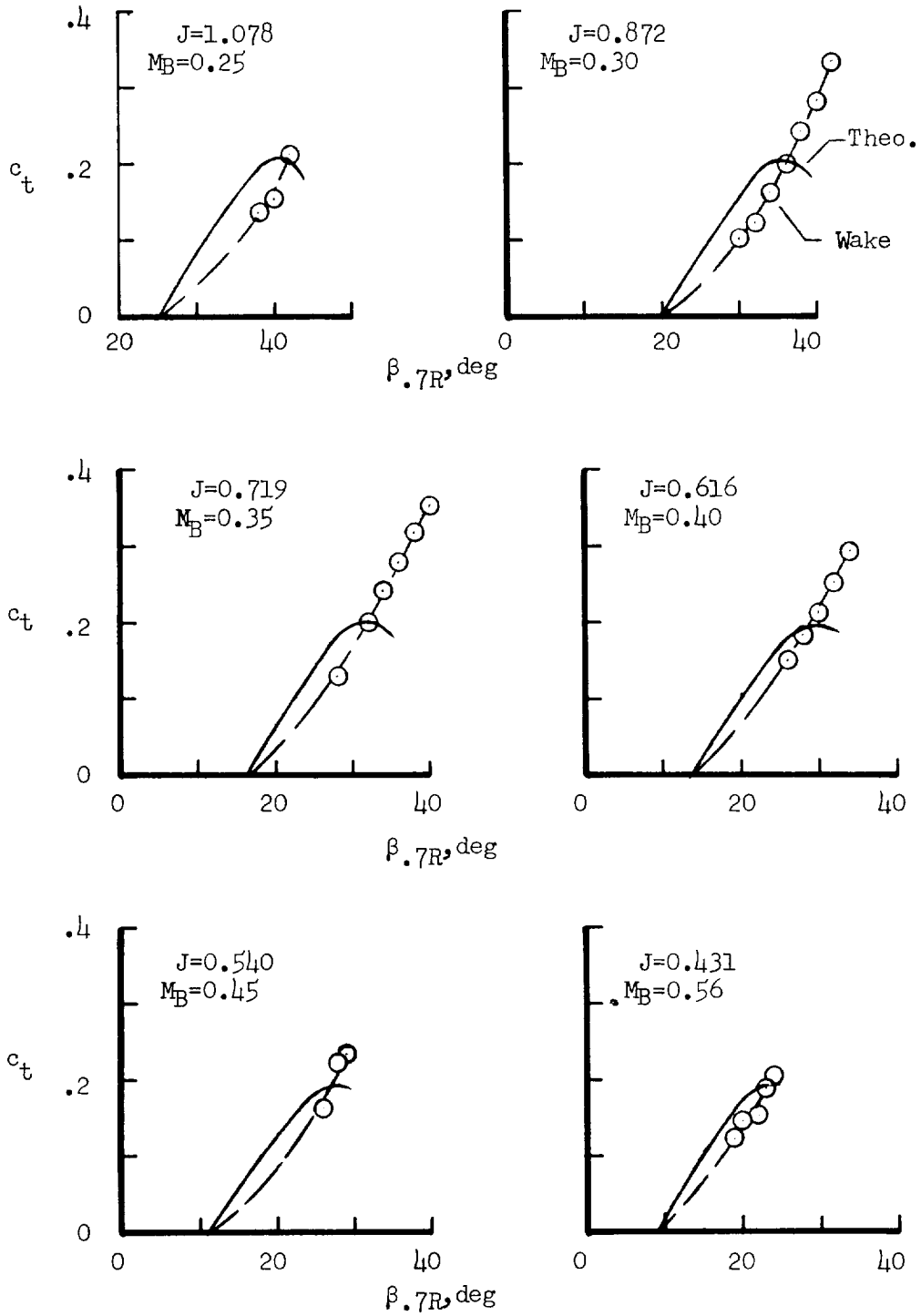

(b) V_∞ = 143.8 fps; x = 0.58

Figure 14.- Continued.

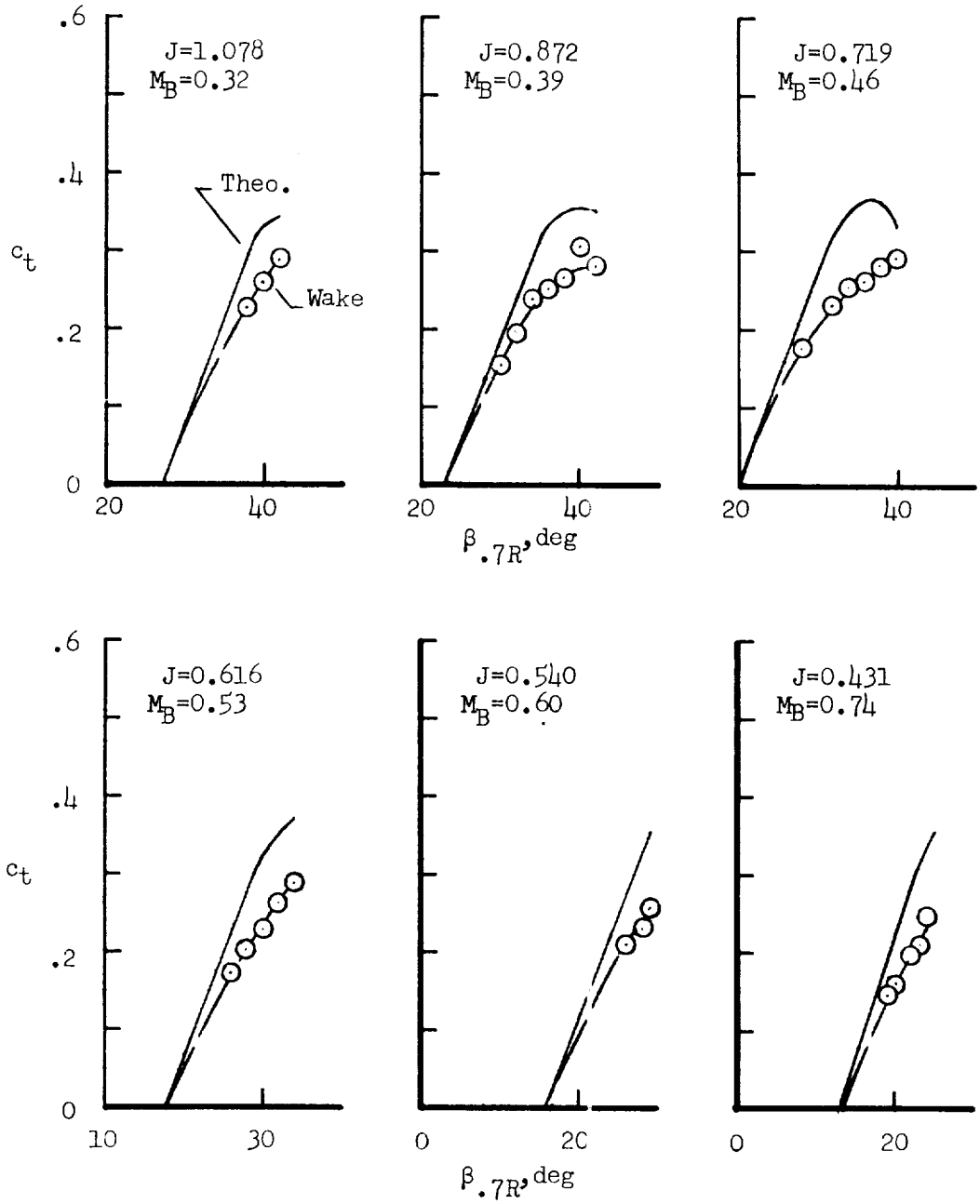

(c) V_∞ = 143.8 fps; :: = 0.78

Figure 14.- Concluded.

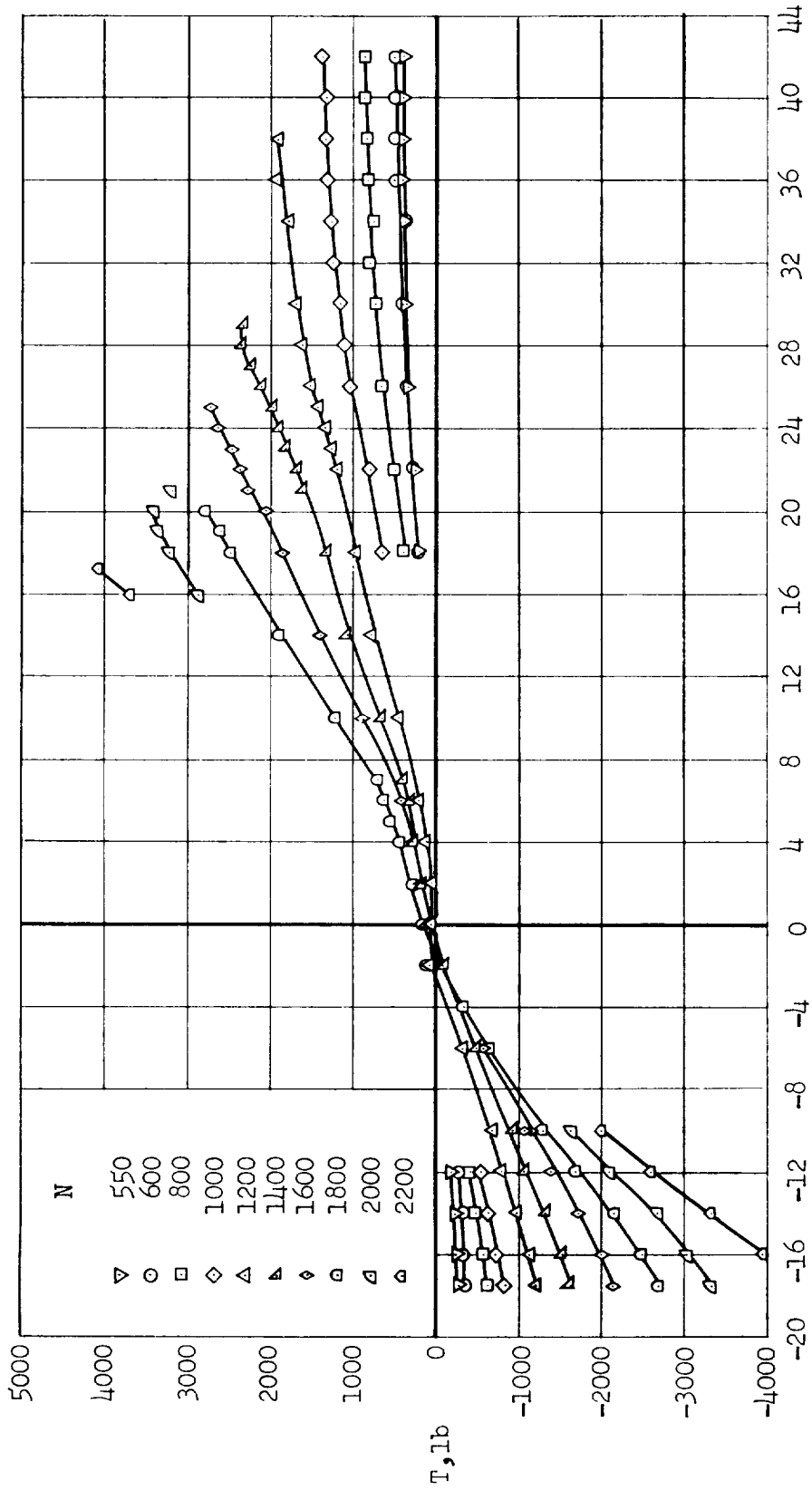

(a) Thrust characteristics; $V_\infty \sim 0$ fps.

Figure 15.- Thrust and power characteristics for constant forward velocity; $\alpha_G = 0^\circ$.

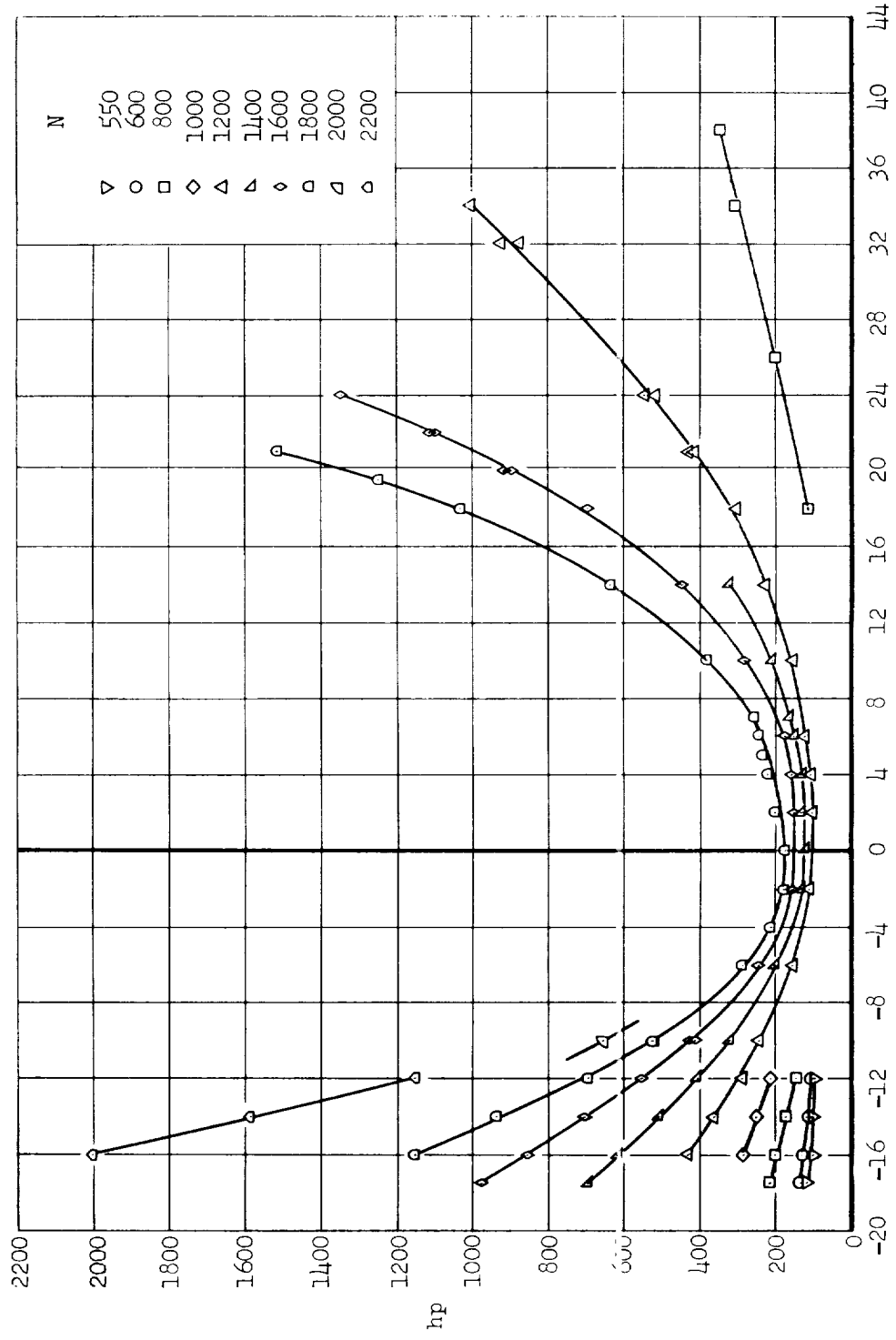

(b) Power characteristics; $V_\infty \sim 0$ fps.

Figure 15.- Continued.

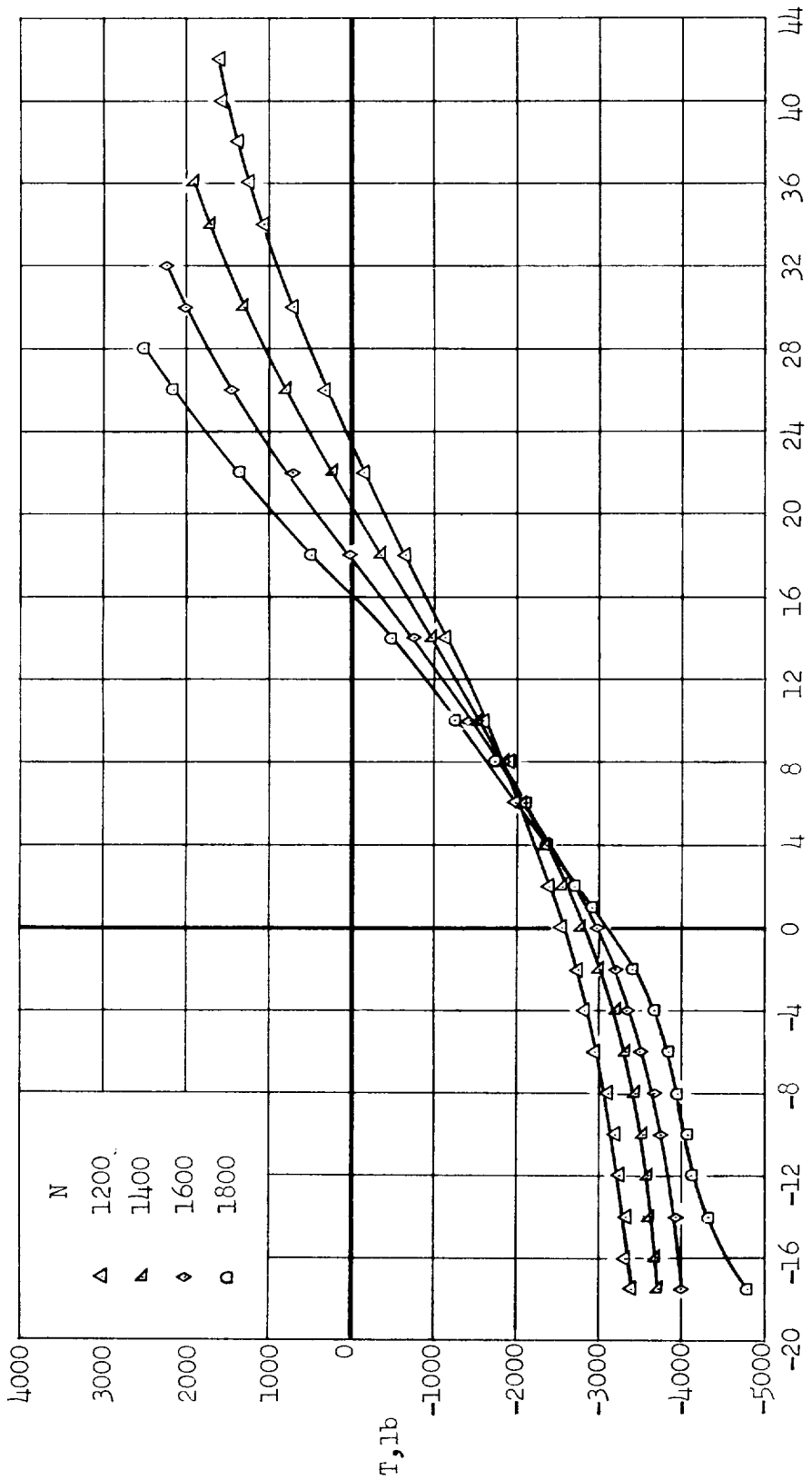

(c) Thrust characteristics; V_∞ = 183.5 fps.

Figure 15.- Continued.

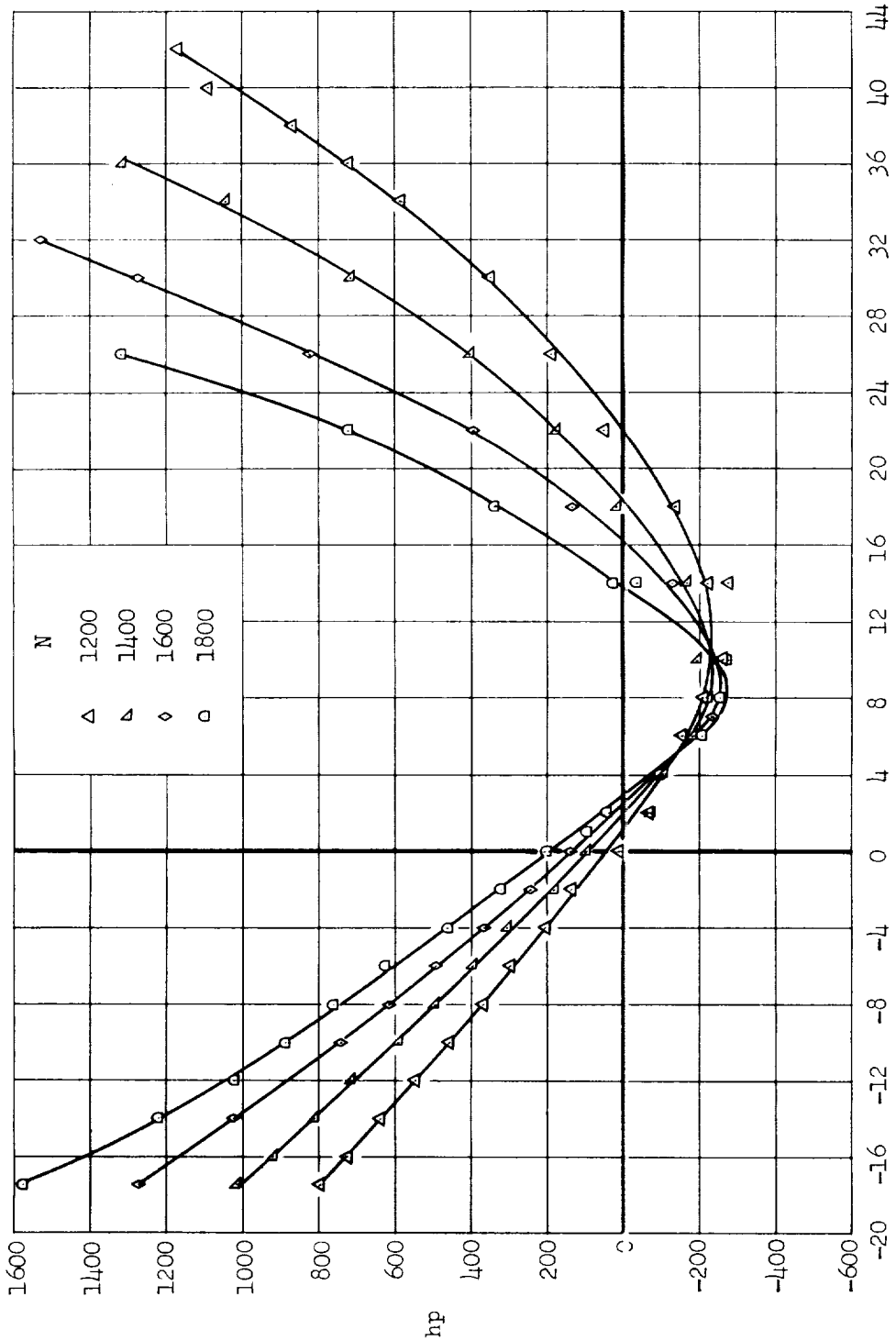

(d) Power characteristics; V_∞ = 183.5 fps.

Figure 15.- Concluded.

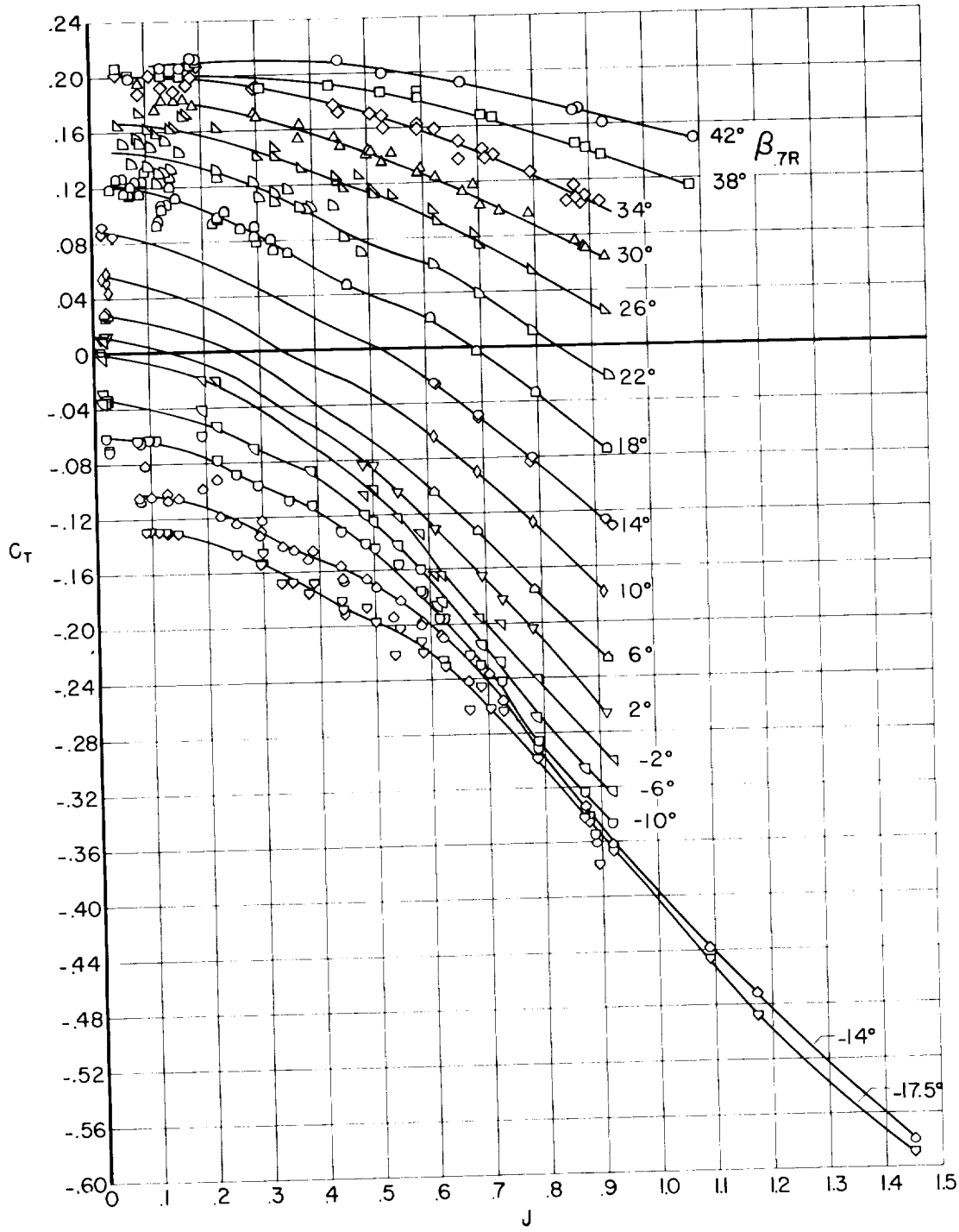

(a) Thrust coefficient, C_T.

Figure 16.- Thrust and power coefficients as a function of advance ratio; $\alpha_G = 0^\circ$.

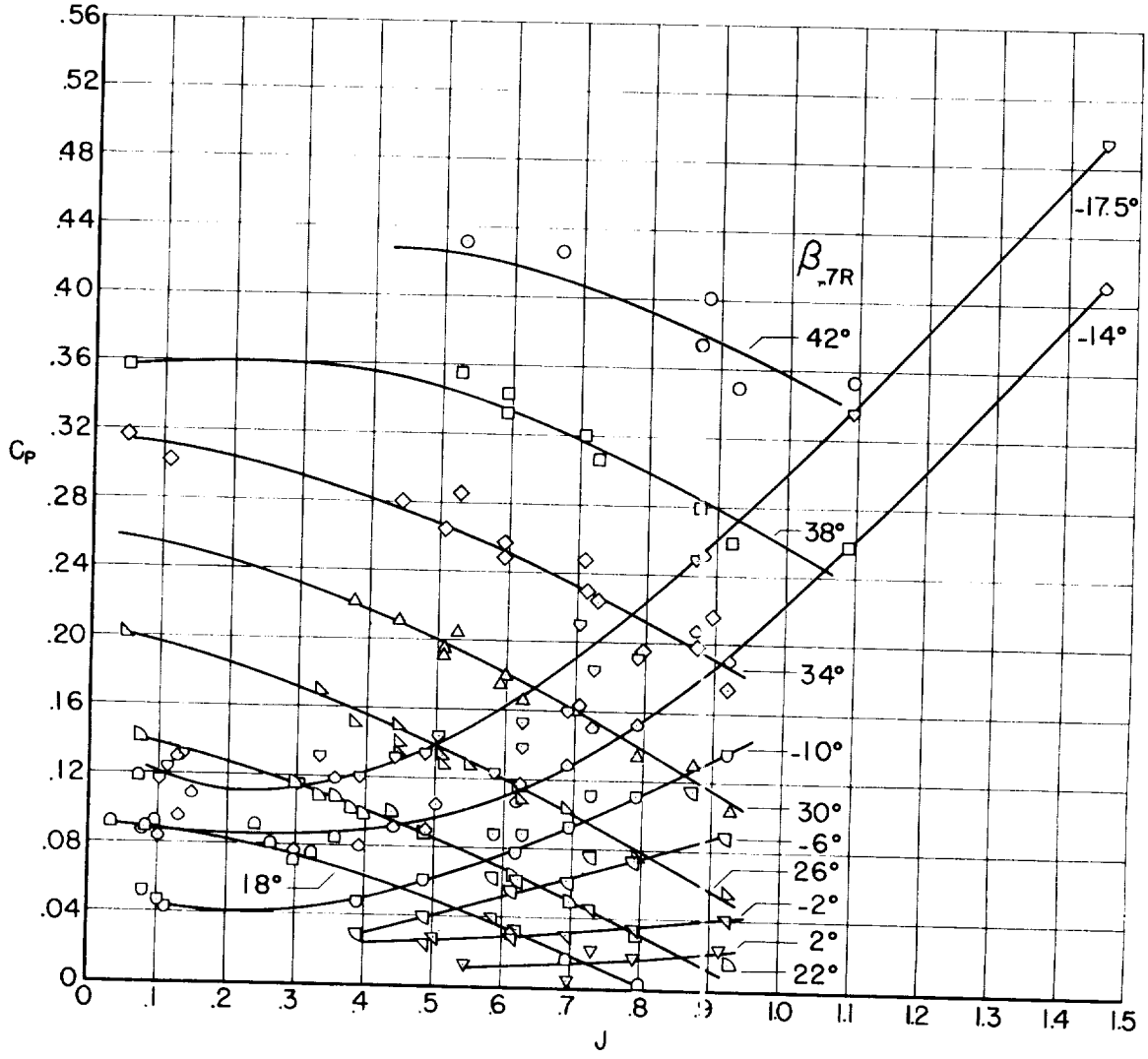

(b) Power coefficient, C_P.

Figure 16.- Concluded.

NASA - Langley Field, Va.